國 立 交 通 大 學

光 電 工 程 研 究 所

碩士論文

使用光迴路之高速長距離波長多工傳輸系統之

研究平台

The Research Platform of High-Speed Long-Haul WDM

Transmission System Using Circulating Loop

研 究 生：連偉志

指導教授：祁　甦 教授

陳智弘 教授

中 華 民 國 九 十 三 年 六 月

使用光迴路之高速長距離波長多工傳輸系統之研究平台

學生：連偉志　　指導教授：祁　甦　教授

陳智弘　教授

國立交通大學光電工程研究所碩士班

摘要

高速長距離波長多工光纖傳輸系統帶給我們令人驚歎的多彩生活。其中，波長多工是大幅增加傳輸量最值得注意的技術之一。我們架設一個使用光迴路之高速長距離波長多工傳輸系統的研究平台來瞭解並研究長距離系統。它包含了八個 10Gb/s 頻道及每個五十公里放置的六個摻鉺光纖放大器。整個系統的色散及色散斜率均利用色散補償光纖調整至最小。藉著控制兩個開關，我們讓信號在迴路裡環行設定好的圈數來模擬長距離系統。實驗結果利用光譜、眼圖及位元錯誤率來展現。

The Research Platform of High-Speed Long-Haul WDM Transmission System Using Circulating Loop

Student : Wei-Chih Lien

Advisors : Dr. Sien Chi

Dr. Jyehong Chen

Institute of Electro-Optical Engineering

National Chiao Tung University

ABSTRACT

The high-speed long-haul fiber optic transmission system brings us to a marvelous colorful life. The Wavelength division multiplexing (WDM) is one of the most remarkable technologies to enlarge the capacity of transmission. We set up a research platform of a high-speed long-haul WDM transmission system by using the circulating loop for more realizing and researching the long-haul systems. It includes eight 10Gb/s channels and six erbium-doped fiber amplifiers (EDFA) with 50km amplifier spacing. The dispersion of the platform is also managed to get minimum overall accumulated dispersion and dispersion slope by dispersion-compensating fiber (DCF). By controlling two switches we allow signals to circulate in the loop for designate times to simulate the long-haul transmission. The experiment results are observed by optical spectrum, eye diagram and the bit error rate (BER).

誌謝

Acknowledgements

隨著時間的車輪邁進，碩士生涯終於來到了終點，儘管那黃金似的日子是一去不復返的，但那黃金似的情誼却將永遠閃爍著光芒。感謝馮開明老師、陳智弘老師的提攜扶持、救危解困，若沒有您們的協助，這本論文便無法順利完成，內心的感謝是千言萬語也無法傳達其中一二，請原諒我僅以一聲：「謝謝」回報您們。

一本論文的完成，背後總是許多人的心血結晶，感謝粘芳芳學姐經驗的傳授，彭朋群學長、黃明芳學姐、林玉明學長的關心與幫忙、嘉健和盈傑適時地解決我的疑惑，有時真懷疑你們是不是上天派來的天使，總是恰如其份的推我一把，你們雪中送來的柴火至今仍在我心中散發溫暖地燒著。

除此之外，尚有一干好友使我在研究生涯之外平添許多樂趣，彭瑋仁學長、建宏、宥燁、馥宇、峰生、昭男、宜錦、昱璋、玉棉，有些在我做實驗的當中陪我聊天解悶，有些在平凡的日子中陪我談笑遊玩，容忍我突如其來的痴狂，有些更是陪我踏上新竹的好山好水，領略人生的優美與曲折，若是少了你們的生氣，碩士生涯就不會這麼的令人不捨及動人，很高興有你們的陪伴。

不能或忘的，是父親、母親的關懷體貼，若沒有您們的支持，我也不能無後顧之憂的將大片的青春揮霍，讓年輕的笑顏展放在大學校園，十多年的栽培令我深深受用，而今我將踏出校園，反哺您們的教養之恩。

兩年的研究生涯一晃眼就過了，卻留下滿滿的回憶，載不走的，載不走的，也要使盡力氣扛著，因為不是你們點綴我的生活，而是我點綴了你們的生活，讓日子發光發亮的，是諸位親愛的師友啊。很愉快能有這麼暢快的學生生活，既使我將在這兒劃下暫離的句點，諸位在交大校園的身影我會謹記於心的。

CONTENTS

List of Figures

CHAPTER 1

Introduction

1.1 The Importance of DWDM and EDFA

An important application of fiber-optic communication links is for enhancing the capacity of telecommunication networks worldwide. Indeed, it is this application that started the field of optical fiber communications in 1977 and has propelled it since then by demanding systems with higher and higher capacities.

For long-haul fiber links forming the backbone of the core of a telecommunication network, the role of WDM is simply to increase the total bit rate. The bit rate was limited to 10Gb/s or less until 1995 because of the limitations imposed by the dispersive and nonlinear effects and by the speed of electronic components. Since then, transmission of multiple optical channels over the same fiber has provided a simple way for extending the system capacity be beyond Tb/s.

The low-loss region of the state-of -the-art “dry” fibers(e.g. fibers with reduced OH-absorption near 1.4um) extends over 300nm in the wavelength region covering 1.3~1.6um. The minimum channel spacing can be as small as 50GHz for 40 Gb/s channels. Since 750 channels can be accommodated over the 300nm bandwidth, the resulting effective bit rate can be as large as 30Tb/s. High capacity WDM fiber links require many high-performance components, such as transmitters integrating multiple DFB lasers, large-bandwidth constant-gain amplifiers, and so on.

Amplifiers are especially valuable for WDM light wave systems as they can amplify many channels simultaneously. Optical amplifiers solve the loss problem but they add noise and worsen the impact of fiber dispersion and nonlinearity since signal degradation keeps on accumulating over multiple amplification stages.

The potential transmission capacity of long systems that use EDFA repeaters was

understood early on [1] [2]. EDFA have become an integral part of almost all fiber-optic communication systems installed after 1995 because of their excellent amplification characteristics such as low insertion loss, high gain, large bandwidth, low noise, and low crosstalk. The employment of EDFA in WDM systems after 1995 revolutionized the field of fiber-optic communications and led to lightwave systems with capacities exceeding 1 Tb/s. The first long-haul EDFA system were TAT-12/13 installed in 1996 with a single 5Gb/s optical signal [3], twice the capacity of the most advanced digital regenerator based undersea fiber optic system at that time.

The gain provided by them is nearly polarization insensitive. Moreover, the inter-channel crosstalk that cripples semiconductor optical amplifier (SOA) because of the carrier-density modulation occurring at the channels spacing dose not occur in EDFA. The reason is related to the relatively large value of carrier lifetime (about 10ms) compared with the one in SOA (<1ns). The sluggish response of EDFA ensures that gain cannot be modulated at frequencies much large than 10 kHz. [4]

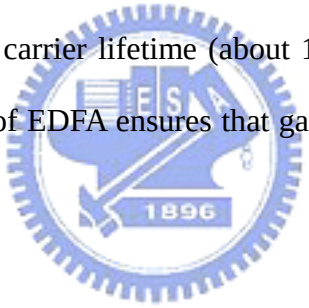

1.2 Objective

Our objective is to set up a loop experiment for studying of the long haul transmission issues. Circulating loop experiment has been performed since the late 1970's. A recent renewed interest in circulating loop experiment has been fueled by R&D of OC-192/STM-64 rate (9.95328Gb/s) transmission systems, dispersion compensating systems, Soliton transmission systems, EDFA based systems, and WDM systems. Circulating loop experiment allows designers to simulate long-haul transmission system with just a fraction of the overall system hardware (fiber, optical amplifiers, filters, etc.). Designers benefit from reduced setup size, complexity, and cost. Circulating loop experiments yield valuable information on the full system BER, eye diagram shape, dispersion, signal to noise power ratio (SNR), and interchannel interaction of a WDM system. For reducing cost the loop

experiment is a good substitution compared to the real long-haul transmission lightwave system.

The circulating loop experiment uses some fiber spans and EDFAs to form a circulation loop and some switches to control how many times the signals circulate. The circulation distance is decided by the circulating times. In other words, the signals are injected into a loop of length L and after they have completed R round-trips they are switched out. The transmission length is RL. [5] Because of the reuse of fiber spans and EDFAs, it decreases the number of components and, of course, the cost. However, effects might appear that would not do so in an equivalent straight line experiment, since effects are averaged over a much shorter length of fiber and a lesser number of amplifiers. In a loop, it does not have the natural statistics of the fiber parameters that it would have in a real system. Hence a loop experiment will tend to emphasize either the very good or the very bad attributes of the fiber used in the loop. Fiber loop experiments were first used by Mollenauer and coworkers to study the long distance transmission of Raman amplified solitons. [6]

I use eight distributed feedback (DFB) lasers as signal sources and an electro-optical (EO) modulator as modulator for coding the non-return to zero (NRZ) modulation format, two acousto-optical (AO) switch as controller of the path of signals, six 50km large effective area (LEAF) fiber spans and six inline EDFAs.

CHAPTER 2

Basic Theory

2.1 Pulse Propagation in Optical Fibers

When short optical pulses with widths ranging from ~10ns to ~10fs propagating inside the fiber, both dispersive and nonlinear effects influence their shape and spectrum. The wave equation is written by

$$\nabla^2\mathbf{E}-\frac{1}{c^2}\frac{\partial^2\mathbf{E}}{\partial t^2}=\mu_0\frac{\partial^2\mathbf{P}_L}{\partial t^2}+\mu_0\frac{\partial^2\mathbf{P}_{NL}}{\partial t^2} \tag{2.1}$$

where $\mathbf{P}_L$ and $\mathbf{P}_{NL}$ are the linear part and nonlinear part of the induced polarization respectively. It is necessary to make several simplifying assumptions in order to solve equation (2.1). First, $\mathbf{P}_{NL}$ is treated as a small perturbation to $\mathbf{P}_L$. Second, the optical field is assumed to maintain its polarization along the fiber length so that a scalar approach is valid. Third, the optical field is assumed to be quasi-monochromatic, i.e., its spectrum, centered at w_0, has a spectral width Δw such that $\Delta w / w_0 \ll 1$. ($w_0 \sim 10^{15} s^{-1}$). In the slowly varying envelope approximation, it is useful to separate the rapidly varying part of the electric field by writing it in the form

$$\mathbf{E}(\mathbf{r},t)=\frac{1}{2}\hat{x}[E(\mathbf{r},t)\exp(-iw_0t)+c.c.] \tag{2.2}$$

where c.c. stands for complex conjugate, $\hat{x}$ is the polarization unit vector of the light assumed to be linear polarized along the x axis. And $\mathbf{E}(\mathbf{r},t)$ is a slowly varying function of time relative to the optical period. The polarization components $\mathbf{P}_L$ and $\mathbf{P}_{NL}$ can also be expressed in a similar way by writing

$$\mathbf{P}_L(\mathbf{r},t)=\frac{1}{2}\hat{x}[P_L(\mathbf{r},t)\exp(-iw_0t)+c.c.], \tag{2.3}$$

$$\mathbf{P}_{NL}(\mathbf{r},t)=\frac{1}{2}\hat{x}[P_{NL}(\mathbf{r},t)\exp(-iw_0t)+c.c.] \tag{2.4}$$

The linear component $\mathbf{P}_L$ can be given by

$$\mathbf{P}_L(\mathbf{r},t) = \varepsilon_0 \int_{-\infty}^{\infty} \chi_{xx}^{(1)}(t-t')E(\mathbf{r},t')\exp[iw_0(t-t')]dt'$$

$$= \varepsilon_0 \int_{-\infty}^{\infty} \tilde{\chi}_{xx}^{(1)}(w)\tilde{E}(\mathbf{r},w-w_0)\exp[-i(w-w_0)t]dw \qquad (2.5)$$

where $\tilde{E}(\mathbf{r},w)$ is the Fourier transform of $E(\mathbf{r},t)$.

The nonlinear component $\mathbf{P}_{NL}$ can be reduced to

$$\mathbf{P}_{NL}(\mathbf{r},t) = \varepsilon_0 \chi^{(3)} \vdots \mathbf{E}(\mathbf{r},t)\mathbf{E}(\mathbf{r},t)\mathbf{E}(\mathbf{r},t) \qquad (2.6)$$

In general, both electrons and nuclei respond to the optical field in a nonlinear manner. The nuclei response is inherently slower compared with the electronic response. For silica fibers the vibrations of Raman response occurs over a time scale 60-70fs. Thus equation (2.6) is approximately valid for pulse widths >1ps since the assumption of instantaneous nonlinear response amounts for neglecting the contribution of molecular vibrations to $\chi^{(3)}$. When equation (2.2) is substituted in equation (2.6), $\mathbf{P}_{NL}(\mathbf{r},t)$ is founded to have term oscillating at w_0 and another term oscillating at the third-harmonic frequency $3w_0$. The latter term is generally negligible in optical fibers. By making use of (2.4), $\mathbf{P}_{NL}(\mathbf{r},t)$ is given by

$$\mathbf{P}_{NL}(\mathbf{r},t) = \varepsilon_0 \varepsilon_{NL} \mathbf{E}(\mathbf{r},t) \qquad (2.7)$$

where ε_{NL} is the nonlinear contribution to the dielectric constant and is defined by

$$\varepsilon_{NL} = \frac{3}{4}\chi_{xxxx}^{(3)} \left|E(\mathbf{r},t)\right|^2 \qquad (2.8)$$

To obtain the wave equation for the slowly varying amplitude $E(\mathbf{r},t)$, it is more convenient to work in the Fourier domain. By substituting equation (2.2)-(2.4) in equation (2.1), the Fourier transform $\tilde{E}(\mathbf{r},w-w_0)$, defined by

$$\tilde{E}(\mathbf{r},w-w_0) = \int_{-\infty}^{\infty} E(\mathbf{r},t)\exp[i(w-w_0)t]dt \qquad (2.9)$$

is found to satisfy

$$\nabla^2\tilde{E} + \varepsilon(w)k_0{}^2\tilde{E} = 0 \tag{2.10}$$

where $k_0 = w/c$ and

$$\varepsilon(w) = 1 + \tilde{\chi}_{xx}{}^{(1)}(w) + \varepsilon_{NL}$$

(2.11)

is the dielectric constant. The dielectric constant can be used to define the refractive index $\tilde{n}$ and the absorption coefficient $\tilde{\alpha}$. However, both $\tilde{n}$ and $\tilde{\alpha}$ become intensity dependent because of ε_{NL}. It is customary to introduce

$$\tilde{n} = n + n_2|E|^2 \tag{2.12}$$

$$\tilde{\alpha} = \alpha + \alpha_2|E|^2 \tag{2.13}$$

Using $\varepsilon = (\tilde{n} + i\tilde{\alpha}/2k_0)^2$ and (2.8) and (2.11), the nonlinear index coefficient n_2 and the two-photon absorption coefficient α_2 are given by

$$n_2 = \frac{3}{8n}\mathrm{Re}(\chi_{xxxx}{}^{(3)}) \tag{2.14}$$

$$\alpha_2 = \frac{3w_0}{4nc}\mathrm{Im}(\chi_{xxxx}{}^{(3)}) \tag{2.15}$$

Since α_2 is relatively small for silica fibers, $\tilde{\alpha} \approx \alpha$, equation (2.10) can be solved using the method of separation of variables. If we assume a solution of the form

$$\tilde{E}(\mathbf{r}, w - w_0) = F(x, y)\tilde{A}(z, w - w_0)\exp(i\beta_0 z) \tag{2.16}$$

where $\tilde{A}(z, w - w_0)$ is a slowly varying function of z and β_0 is the propagation constant to be determined later, equation (2.10) leads to the following two equations for $F(x, y)$ and $\tilde{A}(z, w - w_0)$:

$$\frac{\partial^2 F}{\partial x^2} + \frac{\partial^2 F}{\partial y^2} + [\varepsilon(w)k_0{}^2 - \tilde{\beta}^2]F = 0 \tag{2.17}$$

$$2i\beta_0\frac{\partial\tilde{A}}{\partial z} + (\tilde{\beta}^2 - \tilde{\beta}_0{}^2)\tilde{A} = 0 \tag{2.18}$$

In obtaining equation (2.18), we have neglected the second derivative $\frac{\partial^2 \tilde{A}}{\partial z^2}$ since $\tilde{A}(z,w)$ is assumed to be a slowly varying function of z. The propagation constant $\tilde{\beta}$ is determined by solving the eigenvalue equation (2.17) for the fiber modes. The dielectric constant $\varepsilon(w)$ in equation (2.17) can be approximated by

$$\varepsilon = (n+\Delta n)^2 = n^2 + 2n\Delta n \tag{2.19}$$

where Δn is a small perturbation given by

$$\Delta n = n_2 |E|^2 + \frac{i\alpha}{2k_0} \tag{2.20}$$

Equation (2.17) can be solved by using first-order perturbation theory. [7] We first solve it by replacing ε by n^2 and obtain the modal distribution $F(x,y)$ and the corresponding propagation constant $\beta(w)$. For a single-mode fiber, $F(x,y)$ corresponds to the modal distribution of the fundamental fiber mode HE_{11}. We then include the effect of Δn in equation (2.17). In the first-order perturbation theory, Δn does not affect the modal distribution $F(x,y)$. However, the eigenvalue $\tilde{\beta}$ is given by

$$\tilde{\beta}(w) = \beta(w) + \Delta\beta \tag{2.21}$$

where

$$\Delta\beta = \frac{k_0 \int_{-\infty}^{\infty}\int_{-\infty}^{\infty} \Delta n |F(x,y)|^2 \, dxdy}{\int_{-\infty}^{\infty}\int_{-\infty}^{\infty} \Delta n |F(x,y)|^2 \, dxdy} \tag{2.22}$$

This step completes the formal solution of equation (2.1) to the lowest order in perturbation $\mathbf{P}_{NL}$. Using equation (2.2) and equation (2.12) (2.13), the electric field $\mathbf{E}(\mathbf{r},t)$ is given by

$$\mathbf{E}(\mathbf{r},t) = \hat{x}\frac{1}{2}\{F(x,y)A(z,t)\exp[i(\beta_0 z - w_0 t)] + c.c.\} \tag{2.23}$$

The Fourier transform $\tilde{A}(z, w-w_0)$ of the slowly varying amplitude $A(z,t)$ satisfies equation (2.18) which can be written as

$$\frac{\partial \tilde{A}}{\partial z} = i[\beta(w) + \Delta\beta - \beta_0]\tilde{A} \tag{2.24}$$

where equation (2.21) and approximated $\tilde{\beta}^2 - \beta_0^{\,2}$ by $2\beta_0(\tilde{\beta} - \beta_0)$. The inverse Fourier transform of equation (2.24) provides us the propagation equation for $A(z,t)$. For this purpose it is useful to expand $\beta(w)$ in a Taylor series about the carrier frequency w_0,

$$\beta(w) = \beta_0 + (w - w_0)\beta_1 + \frac{1}{2}(w - w_0)^2\beta_2 + \frac{1}{6}(w - w_0)^3\beta_3 + \ldots \tag{2.25}$$

where

$$\beta_n = \left(\frac{d^n\beta}{dw^n}\right)_{w=w_0} \tag{2.26}$$

The cubic and higher-order terms in the expansion are generally negligible if the spectral width $\Delta w \ll w_0$. The neglect is consistent with the quasi-monochromatic assumption used in the derivation of equation (2.24) and limits its validity to pulse widths $\geq$ 0.1ps. If $\beta_2 = 0$ for some specific values of w_0 (in the vicinity of the zero-dispersion wavelength of the fiber), it may be necessary to include the cubic term.

We substitute equation (2.25) in equation (2.24) and take the inverse Fourier transform by using

$$A(z,t) = \frac{1}{2\pi}\int_{-\infty}^{\infty} \tilde{A}(z, w - w_0)\exp[-i(w - w_0)t]dw \tag{2.27}$$

During the Fourier-transform operation $w - w_0$ is replaced by the differential operator $i(\partial/\partial t)$ and the result is

$$\frac{\partial A}{\partial z} = -\beta_1\frac{\partial A}{\partial t} - \frac{i}{2}\beta_2\frac{\partial^2 A}{\partial t^2} + i\Delta\beta A \tag{2.28}$$

The term with $\Delta\beta$ includes the effect of fiber loss and nonlinearity. By using equation (2.20) and equation (2.22), $\Delta\beta$ can be evaluated and substituted in equation (2.27). The result is

$$\frac{\partial A}{\partial z} + \beta_1\frac{\partial A}{\partial t} + \frac{i}{2}\beta_2\frac{\partial^2 A}{\partial t^2} + \frac{\alpha}{2}A = i\gamma|A|^2 A \tag{2.29}$$

where the nonlinear parameter γ is defined by

$$\gamma = \frac{n_2 w_0}{c A_{eff}}$$

In obtaining equation (2.29) the pulse amplitude A is assumed to be normalized such that $|A|^2$ represents the optical power. The quantity $\gamma|A|^2$ is then measured in units of m^{-1} if n_2 is expressed in units of m^2/W .Usually n_2 is about $2.6\times10^{-20} m^2/W$. The parameter A_{eff} is known as the effective core area.

Equation (2.29) describes the propagation of an optical pulse in single-mode fibers. It is sometimes referred to as the nonlinear *Schrödinger* equation since it can be reduced to that equation under certain conditions. It includes the effects of fiber loss through α , of chromatic dispersion through β_1 and β_2 , and of fiber nonlinearity through γ . The pulse envelope moves at the group velocity $v_g = 1/\beta_1$ while group velocity dispersion is accounted for by β_2 . [8]

2.2 Basic Concepts of Chain Amplifiers

The simplest way to analyze a cascade of optical amplifiers is to assume that all amplifiers have the same gain and that the loss between amplifiers exactly matches the amplifier gain. The signal output power at the end of the chain is assumed to be equal to the signal input power at the beginning of the chain, a relatively accurate assumption when the ASE generated is small compared to the signal power.

In fact, the ASE is growing at the expense of the signal in saturated amplifier chains, but this does not obviate the main conclusions of the following discussion. Each amplifier generates an equal amount of ASE as the other amplifier, and this ASE propagates transparently to the output of the chain, much as the signal does. Thus, the ASE at the output of the chain is linear addition of the ASE generated by each amplifier. The SNR at the output of the amplifier chain in then obtained by replacing the inversion parameter n_{sp} by Nn_{sp} where N is the number of the amplifiers in the chain and

$$n_{sp} = \frac{\sigma_e(\lambda)N_2}{\sigma_e(\lambda)N_2 - \sigma_a(\lambda)N_1} \tag{2.30}$$

where σ_e and σ_a are the emission and absorption cross section of erbium-doped fiber respectively, and N_1 and N_2 are the population in low and high level of erbium-doped fiber respectively.

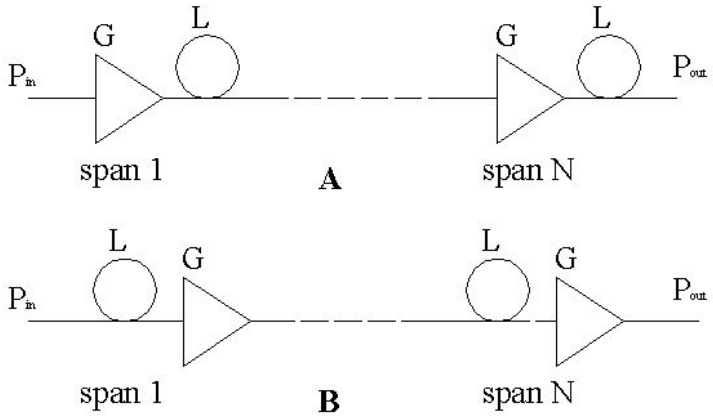

Figure 2.1 Two cases of amplifier chains.

We consider the case of the configuration of Fig. 2.1 A, which corresponds to an amplifier chain where the input power P_{in} to the amplifiers is independent of the amplifier gain G or the span loss L. We compute the SNR under the assumption that it is determined by signal-spontaneous beat noise. The SNR at the output of the amplifier chain can be written, as noted above, using the fact that the ASE at the output of the amplifier chain is N times the ASE generated by one amplifier. The signal input to the receiver is P_{in} / L , when GL=1

$$SNR_A = \frac{P_{in}}{4Nn_{sp}h\nu B_e(G-1)L} \tag{2.31}$$

where B_e is the electrical bandwidth. The total gain G_{tot} and loss L_{tot} of the system are given by

$$G_{tot} = \frac{1}{L_{tot}} = G^N = \frac{1}{L^N} \tag{2.32}$$

The SNR after the last amplifier can then be written as

$$SNR_A = \frac{P_{in}}{4n_{sp}h\nu B_e}\frac{G_{tot}^{1/N}}{(G_{tot}^{1/N}-1)N} \tag{2.33}$$

Equation (2.33) yields the result that the SNR is maximized when N=1. In other words, there should be only one amplifier and the amplifier spacing should be the longest possible. From the point of view that each amplifier adds noise, it makes sense that we find that the minimum number of amplifies gives the best system performance.

We now turn our attention to the system in Fig. 2.1 B, this configuration corresponds to a situation where the amplifier output power is held constant, since whatever the span loss L, the amplifier will be selected to have a gain G such that the output of each lossy span an amplifier unit is equal to the signal input power P_{in}, to ensure a fully transparent chain. The SNR at the output of the amplifier chain is given by

$$SNR_B = \frac{P_{in}}{4Nn_{sp}h\nu B_e(G-1)} \tag{2.34}$$

The difference with respect to equation (2.33) is that here P_{in} is measured at the beginning of the chain, whereas in equation (2.33) P_{in} was measured at the input to the amplifier. Similarly to the derivation of SNR_A, we can write

$$SNR_B = \frac{P_{in}}{4n_{sp}h\nu B_e}\frac{1}{(G_{tot}^{1/N}-1)N} \tag{2.35}$$

where the P_{in} of the signal-spontaneous beat noise is just calculated before first amplifier. Equation (2.35) can be written as

$$SNR_B = \frac{P_{in}}{4n_{sp}h\nu B_e}\frac{1}{\ln G_{tot}}\frac{\ln G}{(G-1)} \tag{2.36}$$

In this case the SNR is improved by increasing the number of amplifiers and reducing the gain G correspondingly. In the limit where the number of amplifier goes to infinity the SNR is maximized and is equal to

$$SNR_B(\max) = \frac{P_{in}}{4n_{sp}h\nu B_e}\frac{1}{\ln G_{tot}} \tag{2.37}$$

This result can be understood from the fact that as we decrease the amplifier gain, the

amplifier input power increases since the preceding span is now shorter and its loss less. Any loss prior to the input of an amplifier degrades the noise figure and the output SNR.

How do we resolve the apparent contradiction between the conceptual conclusions of cases A and B? The maximum SNR for case A is the high SNR for either configuration. But it is not a practical construction to use just one amplifier for the chain loss. In addition, the onset of nonlinear effects above a certain power level limits the output power to be launched in the chain. Real life systems are similar to the configuration B where amplifier output power is held constant. In this case short amplifier spacings are desirable. Given the economic cost of amplifiers, practical systems use amplifier spacings as long as possible while still maintaining a minimum system SNR for low error rate detection.

The discussion above we consider the expression for the SNR with a continuous signal P_{in}. For configuration B, a random pattern of 1s and 0s, and an infinite extinction ratio, one can derive, given that the signal-spontaneous noise is only present during the 1s, that the electrical SNR is given by

$$SNR_B = \frac{P_{in}}{2n_{sp}h\nu B_e(G-1)} = \frac{B_o}{B_e} SNR_{opt} \tag{2.38}$$

where P_{in} is the average optical power and B_o is the optical bandwidth.

The optical SNR is often used to quickly characterize the system properties of a cascaded amplifier chain, since the SNR can be directly measured on an optical spectrum analyzer.

The noise figure for a system consisting of a chain of optical amplifiers can be computed from the noise figure for an individual amplifier. Consider a system of N amplifiers where SNR_i denotes the SNR after amplifier I, and each amplifier provides a gain G to exactly compensate the span loss. The overall noise figure (F) of the system is given by

$$F_{sys} = \frac{SNR_0}{SNR_N} = \frac{SNR_0}{SNR_1}\frac{SNR_1}{SNR_2}\cdots\frac{SNR_{N-1}}{SNR_N} \tag{2.39}$$

where SNR_0 is the SNR at the input of the system immediately after the transmitter and

prior to the first span of fiber. The SNR ratios are the noise figures of each amplifier multiplied by 1/L since the amplifier noise figure is defined by the SNR's immediately prior and after the amplifier. Each SNR_i is separated form the following amplifier by a span with loss L, hence we obtain for the system noise figure, in logarithmic units

$$F_{sys} = GF_1 + GF_2 + ... + GF_N = NGF \tag{2.40}$$

assuming all the amplifiers have an equal noise figure and G=L, and noise figure with shot noise without considering the ASE and signal-spontaneous beat noise. The SNR degradation in a cascaded amplifier transparent chain is seen to be linear with the number of amplifiers. An interesting result can be derived when G and L are different, as is the case for a multistage amplifier constructed by piecing together several amplifiers. Equation (2.40) is then written more generally as

$$F_{sys} = \frac{F_1}{L_1} + \frac{F_2}{L_1 G_1 L_2} + ... + \frac{F_N}{L_1 G_1 L_2 G_2 ... L_N} \tag{2.41}$$

where L_i and G_i refer to the loss prior to amplifier i and the gain of amplifier i, respectively.[5]

Chapter 3

WDM Source of 10 Gb/s Channels and Key Component of Loop Experiment

3.1 Description of DFB Laser

In WDM systems, we want to carry many multiplexed optical signals on the same fiber. To do this it is important for each signal to have as narrow as spectral width as possible and to be as stable as possible. DFB lasers are one answer to this requirement. The idea is that you put a Bragg grating in the laser cavity of an index-guided Fabry-Perot laser. This is just a periodic variation in the refractive index of the gain region along its length. The presence of the grating causes small reflections to occur at each reflective index change (corrugation). When the period of the corrugations is a multiple of the wavelength of the incident light, constructive interference between reflections occurs and a proportion of the light is reflected. Other wavelengths destructively interfere and therefore cannot be reflected. The effect is strongest when the period of the Bragg grating is equal to the wavelength of light used (first order grating). Mode selectivity of the DFB mechanism results from the Bragg condition: the coupling occurs only for wavelengths λ_B satisfying

$$\Lambda = m(\lambda_B / 2\bar{n}) \tag{3.1}$$

where Λ is the grating period, $\bar{n}$ is the average mode index, and the integer m represents the order of Bragg diffraction. The coupling between the forward and backward waves is strongest for the first-order Bragg diffraction (m=1). So the device will work when the grating period is any small integer multiple of the wavelength. Thus only one mode, the one that conforms to the wavelength of the grating, can be lasing. Early devices using the principle had the grating within the active region and were found to have too much attenuation. As a result the grating was moved to a waveguide layer immediately adjacent to (below) the cavity as shown in Fig. 3.1 (a). The evanescent field accompanying the light wave in the cavity extends

into the adjacent layer and interacts with the grating to produce the desired effect.

In principle a DFB laser does not need end mirrors. The grating can be made strong enough to produce sufficient reflection for lasing to take place. However, in a perfect DFB laser there are actually two lines produced, one at each side of the Bragg wavelength. We only want one line. A way of achieving this and improving the efficiency of the device is to place a high reflectance end mirror at one end of the cavity and either an anti-reflection coating or just a cleaved facet at the output end. In this case the grating does not need to be very strong, just sufficient to ensure that a single mode dominates. The added reflections from the end mirrors act to make the device asymmetric and suppress one of the two spectral lines. Unfortunately, they also act to increase the line width.

Some DFB lasers are constructed with a quarter-wave grating shift in the middle section of the grating to introduce a $\pi/2$ phase shift as show in Fig. 3.1 (b). This phase shift grating introduces a sharp transmission fringe into the grating reflection band as shown in Fig. 3.2. What happens is that the reflected waves from each end of the grating will be out of phase with each other and hence will destructively interfere. The fringe acts to narrow the linewidth of the laser significantly. The output spectrum of light is shown in Fig. 3.3. It shows apparently that the number of output signals can be reduced from two to one by $\pi/2$ phase shift grating. [9]

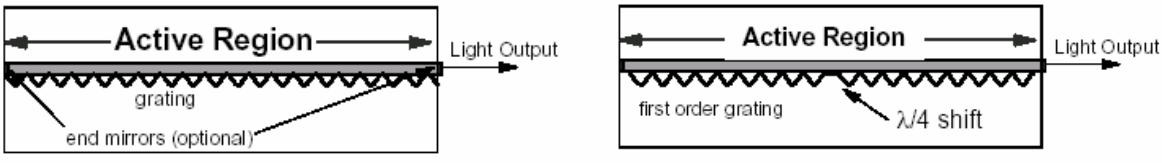

(a) (b)

Figure 3.1 Structure of DFB laser (a) without $\pi/2$ (b) with $\pi/2$ phase shift grating.

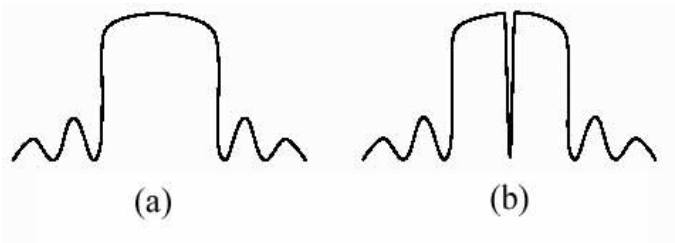

Figure 3.2 Reflection Characteristics (a) without phase shift grating (b) with phase shift grating.

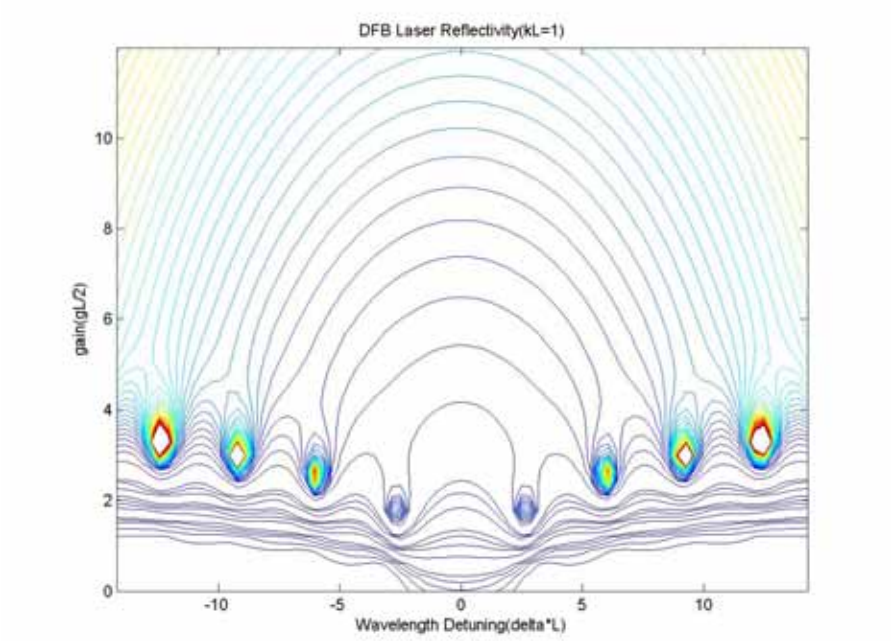

(a)

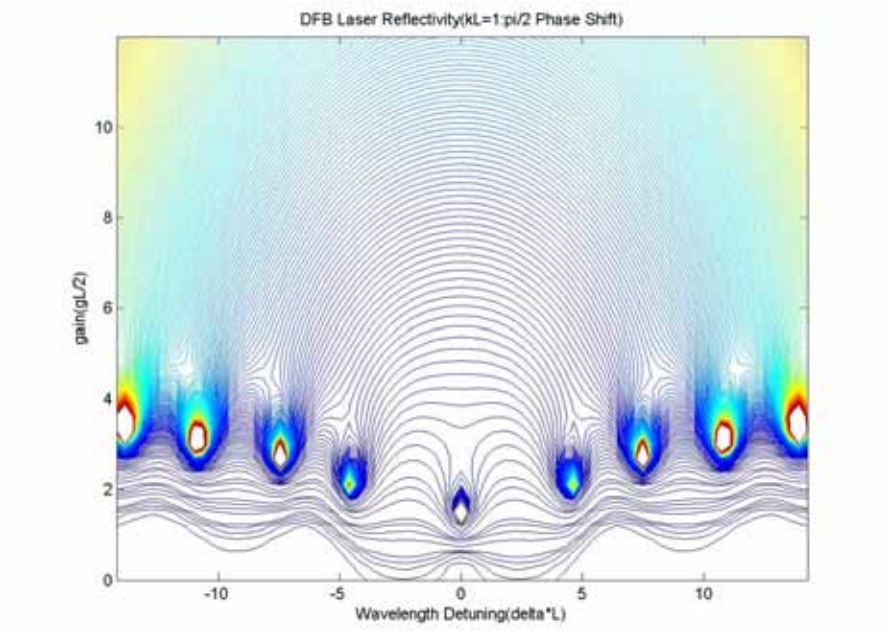

(b)

Figure 3.3 Reflectivity Spectrum (a) without $\pi/2$ (b) with $\pi/2$ phase shit grating.

3.2 Electro-Optical Effect

In certain types of crystals, the application of an electric field results in a change in both the dimensions and orientation of the index ellipsoid. This is referred to as the electro-optic effect. The electro-optic effect affords a convenient and widely used means of controlling the phase or intensity of the optical radiation. According to the quantum theory of solids, the optical dielectric impermeability tensor η_{ij} depends on the distribution of charges in the crystal. The application of an electric field will result in a redistribution of the bond charges and possibly a slight deformation of the ion lattice. The net result is a change in the optical impermeability tensor. The electro-optic coefficients are defined traditionally as:

$$\eta_{ij}(\mathbf{E}) - \eta_{ij}(0) \equiv \Delta\eta_{ij} = r_{ij}E_k + s_{ijkl}E_kE_l = f_{ijk}P_k + g_{ijkl}P_kP_l \tag{3.2}$$

where $\mathbf{E}$ is the applied electric field and $\mathbf{P}$ is the polarization field vector. The constants r_{ij} and f_{ijk} are the linear (or Pockels) electro-optic coefficients, and s_{ijkl} and g_{ijkl} are the quadratic (or Kerr) electro optic coefficients. In the above expansion, terms higher than the quadratic are neglected because these higher-order effects are too small for most applications.

The electro-optic coefficients of the $LiNbO_3$ crystal are in the form:

$$\begin{pmatrix} 0 & -r_{22} & r_{13} \\ 0 & r_{22} & r_{13} \\ 0 & 0 & r_{33} \\ 0 & r_{51} & 0 \\ r_{51} & 0 & 0 \\ -r_{22} & 0 & 0 \end{pmatrix} \tag{3.3}$$

We now consider the case when the electric field is along the c axis of the crystal so that the equation of the index ellipsoid can be written as:

$$x^2\left(\frac{1}{n_0^{\,2}} + r_{13}E\right) + y^2\left(\frac{1}{n_0^{\,2}} + r_{13}E\right) + z^2\left(\frac{1}{n_e^{\,2}} + r_{33}E\right) = 1 \tag{3.4}$$

where n_0 and n_e are the ordinary and extraordinary refractive indecies, respectively. Since no mixed terms appear in equation (3.4), the principal axes of the new index ellipsoid remain

unchanged. The lengths of the new semi-axes are:

$$n_x = n_0 - \frac{1}{2} n_o^{\,3} r_{13} E \tag{3.5}$$

$$n_y = n_0 - \frac{1}{2} n_o^{\,3} r_{13} E \tag{3.6}$$

$$n_z = n_e - \frac{1}{2} n_e^{\,3} r_{33} E \,. \tag{3.7}$$

Note that under the influence of the electric field in the direction of c axis, the crystal remains uniaxially anisotropic. If a light beam is propagating along the y axis, the birefringence seen by it is

$$n_z - n_x = (n_e - n_o) - \frac{1}{2}(n_e^{\,3} r_{33} - n_o^{\,3} r_{13}) E \tag{3.8}$$

The phase retardation of this plate is:

$$\Gamma = \frac{w}{c}(n_z - n_x) d = \frac{2\pi}{\lambda}[(n_e - n_o) - \frac{1}{2}(n_e^{\,3} r_{33} - n_o^{\,3} r_{13})]V \tag{3.9}$$

where V is the voltage applied and d is the thickness of crystal. The voltage making the retardation $\Gamma = \pi$ is known as the "half-wave voltage," and is given in the case by:

$$V_\pi = \frac{\lambda}{2[(n_e - n_o) - \frac{1}{2}(n_e^{\,3} r_{33} - n_o^{\,3} r_{13})]} \tag{3.10}$$

The electrically induced birefringence causes a wave incident at y=0 with its polarization along x to acquire a z polarization, which grows with voltage at the expense of the x component until at $V = V_\pi$ and then the polarization becomes parallel to z. If at the output plane one inserts a polarizer at right angles to the input polarization then with the field on, the optical beam passes through unattenuated, the output beam is blocked off completely by the crossed output polarizer. This control of the optical flow serves as the basis of the electro-optic amplitude modulation of light. [10]

3.3 Key component of Loop Experiment

3.3.1 Acousto-Optic Effect

Acousto-optic interaction occurs in all optical mediums when an acoustic wave and a laser beam are present in the medium. When an acoustic wave is launched into the optical medium, it generates a refractive index wave that behaves like a sinusoidal grating. An incident laser beam passing through this grating will diffract the laser beam into several orders as shown in Fig. 3.4.

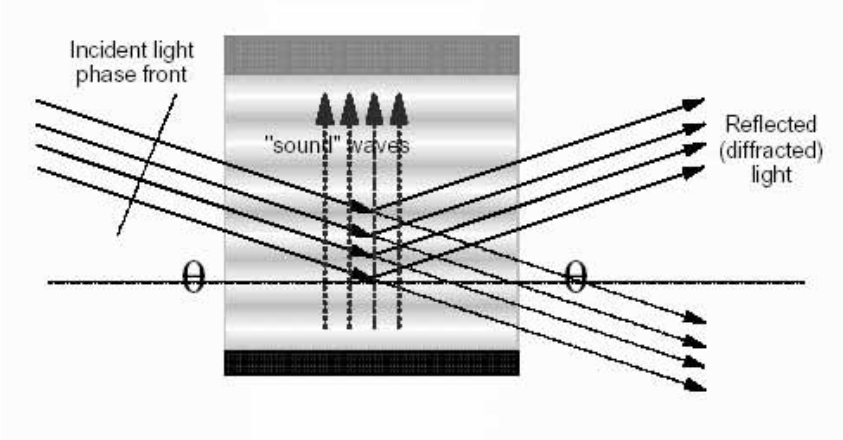

Figure 3.4 Principle of AO effect.

With appropriate design, the first order beam has the highest efficiency. Its angular position is linearly proportional to the acoustic frequency, so that the higher the frequency, the larger the diffracted angle.

$$\theta = \frac{\lambda f_a}{V_a} \tag{3.11}$$

where λ is the optical wavelength, f_a is the acoustic frequency, V_a is the acoustic velocity, and θ is the angle between the incident laser beam and the diffracted laser beam, with the acoustic wave direction propagating at the base of the triangle formed by the three vectors. The intensity of light diffracted (deflected) is proportional to the acoustic power P_{ac}, the material figure of merit M_2, geometric factors (L/H) and inversely proportional to the

square of the wavelength. This is seen in the following equation:

$$D.E. = \eta = \sin^2[\frac{\pi}{\lambda}(\frac{M_2 P_{ac} L}{2H})^{\frac{1}{2}}] \quad (3.12)$$

In the AO interaction, the laser beam frequency is shifted by an amount equal to the acoustic frequency.

The principal performance parameter is the modulation speed which is primarily determined by the transit time, t. The transit time t and the rise time t_r are given by:

$$t = \frac{V}{d} \quad (3.13)$$

$$t_r = 0.85t \quad (3.14)$$

The AO device is be used to shutter the laser beam “on” and “off” by an external digital TTL signal. It must have low insertion loss, low polarization dependency, high extinction ratio, and small rise and fall time to minimize transients. The repetition rate of the switch is a function of the loop delay time. Typical repetition rates are in the kHz range. [11]

Circulating loop experiments require AO switches to have high extinction ratio (>50dB), low polarization dependent loss (<0.5dB), moderate switching speed (~70ns) and low insertion loss (<3dB). A high extinction ratio is especially important on the transmitter switch, since data is launched into the loop for only a small fraction of the experimental period. Light that leaks through this switch during the loop phase looks like optical noise injected every span. Thus light that leaks through the switch trends to corrupt the data signal and diminished the accurate emulation of a straight system. Low loss is important since any attenuation inside the loop looks like a periodic loss in every circulation, which means added noise and/of diminished SNR. Low polarization dependent loss in the optical switch is necessary to prevent high and low polarization loss modes from accumulating in the loop. To perform effective switching, the AO switches should have a short switching time compared to the loop time in the loop. When the AO switches are operated in deflection mode, the frequency of light passing through it is shifted by an amount equal to the RF drive frequency

(MHz). Thus every time the optical signals pass through the loop it incurs a MHz frequency shift. For practical numbers of circulations, this frequency shift is small and does not adversely affect the expected results. [12]

3.3.2 The Gain Flatten of EDFA

The main practical limitation of an EDFA stems from the spectral non-uniformity of the amplifier gain. Even though the gain spectrum of an EDFA is relatively broad, the gain is far from uniform (of flat) over a wide wavelength. As a result, different channels of a WDM signal are amplified by different amounts. This problem becomes quite severe in long-haul systems employing a cascaded chain of EDFAs. The reason is that small variations in the amplifier gain for individual channels grow exponentially over a chain of in-line amplifiers if the gain spectrum is the same for all amplifiers. Even a 0.2dB gain difference grows to 9.6dB over a chain of 48 EDFAs.

The usable bandwidth of inline EDFA can be increased by using passive gain equalizing filters. The idea of gain equalizing filters is designed to approximate the inverse of gain spectrum. Our EDFAs are specially designed and have flat gain spectrum as shown in Fig. 3.5.

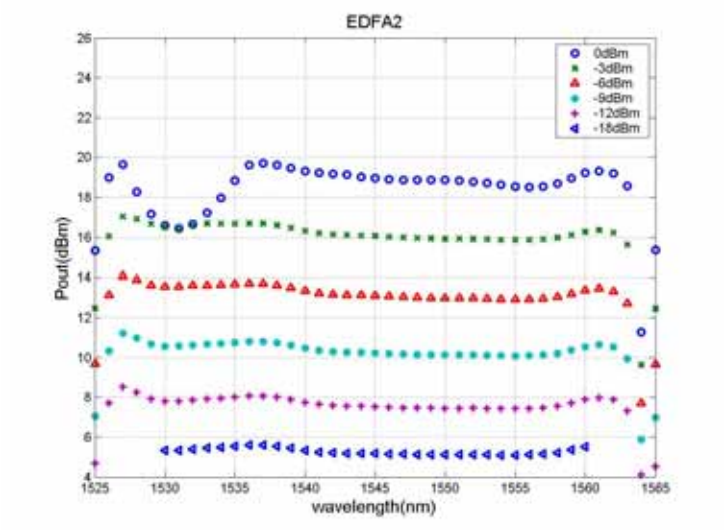

Figure 3.5 Output power versus wavelength of one of the inline EDFAs.

CHAPTER 4

Dispersion Management

4.1 Dispersion Compensation

For long-haul transmission systems, the nonlinear refractive index can couple different signal channels, and can also couple the signal with noise. It will cause the distortion, spectrum broadening and other degradations. If it is operated around the zero dispersion wavelength in fiber, the data signals and the amplifier noise with wavelengths similar to the signal travel at similar velocity. Under these conditions the signal and noise waves have long interaction lengths and can mix together. Especially the NRZ format is affected severely by nonlinearity because it has long interaction lengths. [13] Chromatic dispersion causes different wavelengths to travel at different group velocities in single mode transmission fiber.[8][14] Chromatic dispersion can reduce phase matching, or the propagation distance over which closely spaced wavelengths overlap, and can reduce the amount of nonlinear interaction in the fiber. Thus, in a long undersea system, the nonlinear behavior can be managed by tailoring the accumulated dispersion so that the phase-matching lengths are short, and the end-to-end dispersion is small. The technique has been used in both single channel systems to reduce nonlinear interaction between signal and noise as well as in WDM system. [15]

Before we compensate the dispersion, the bit stream is Fig. 4.1, 4.2. It has peaks in the rising edge and falling edge of the bit stream. And so the eye diagram is distortion seriously. The walkoff can be minimized if the pulse wavelength and the zero dispersion wavelength of the fiber are very close. This is not often a good solution since operating near zero dispersion leads to significant impairment from the phase-matched mixing between the signal and the amplifier noise. In addition, if any optical filter clips the broadened spectrum then pulse distortion will occur in the time domain. In principle, if the total spectrum is

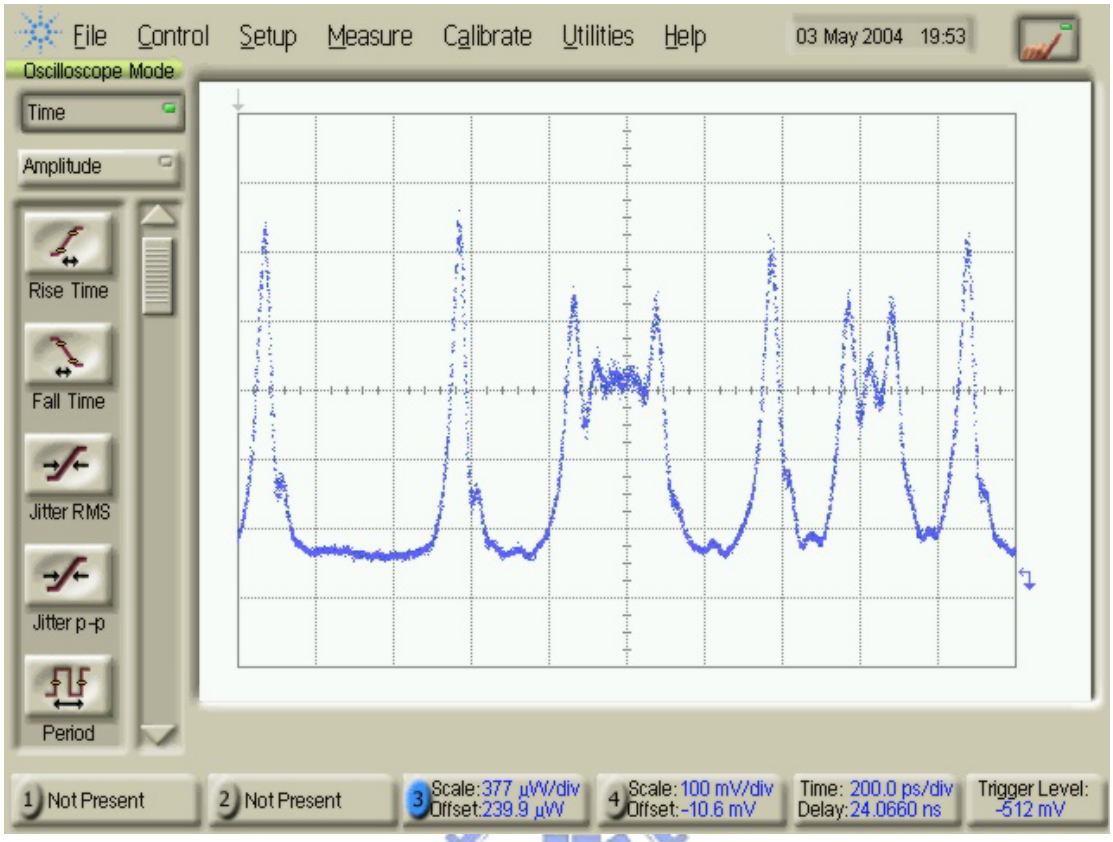

Figure 4.1 The bit stream after 150km.

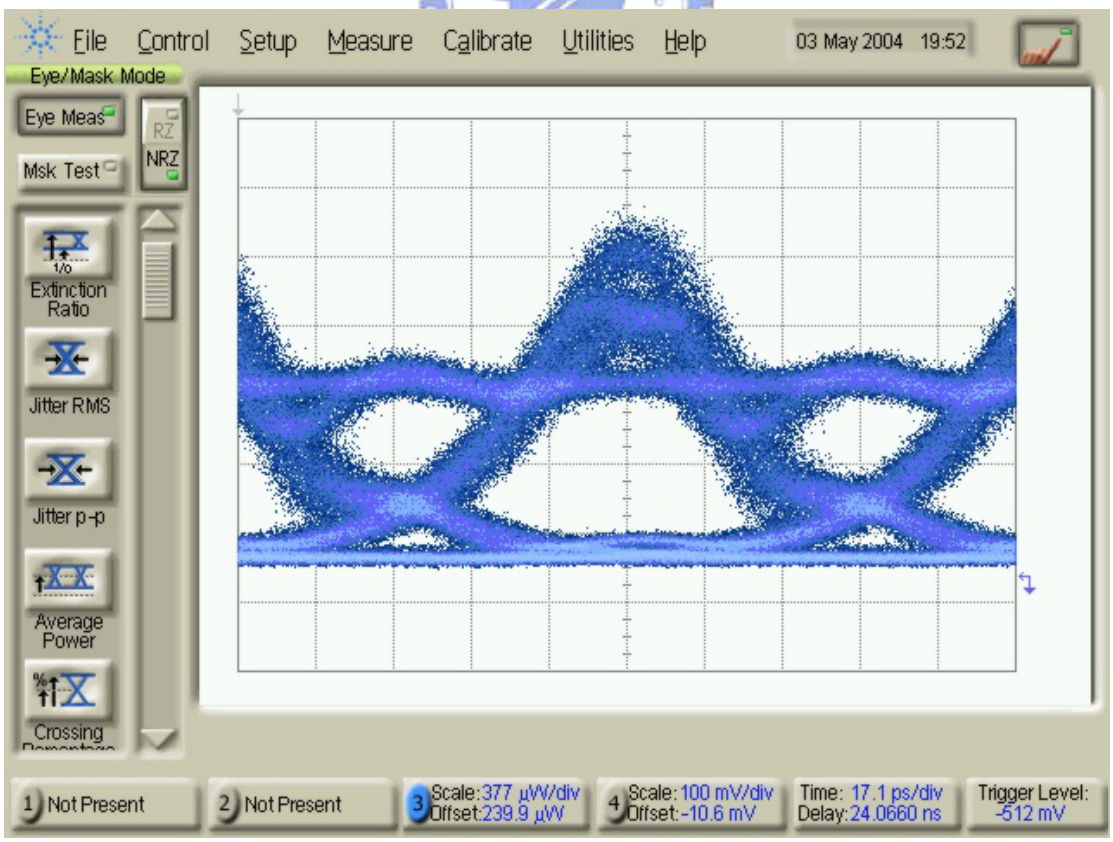

Figure 4.2 The eye diagram after 150km.

admitted to the receiver then no pulse distortion will occur, although this may lead to impairment of the SNR due to the increased ASE noise admitted. Thus, dispersion compensation which null the overall dispersion of the chain can significantly reduce the combined effect of SPM and group velocity dispersion.

There is a brief method to measure the coarse dispersion parameter (D). By use a tunable laser as source when changing its wavelength the final signal bit stream will delay some nanosecond after one loop as show in Fig. 4.3 and 4.4. The quotient of delay time over wavelength variation over transmission length can give the coarse dispersion parameter.

We use two DCFs (D=-86.6231ps/nm/km and loss=0.37dB/km at 1553.33nm) to compensate the accumulated chromatic dispersion. One is 4.37896km and the other is 10.81287km. The dispersion map similar to that is shown in Fig. 4.5. The locally dispersion is rather large but the accumulated total dispersion in each round-trip is near zero as shown in Fig. 4.6. In Fig. 4.6 I measured two times for more accuracy. It can help to walk-off each channel and to eliminate the four-wave mixing.

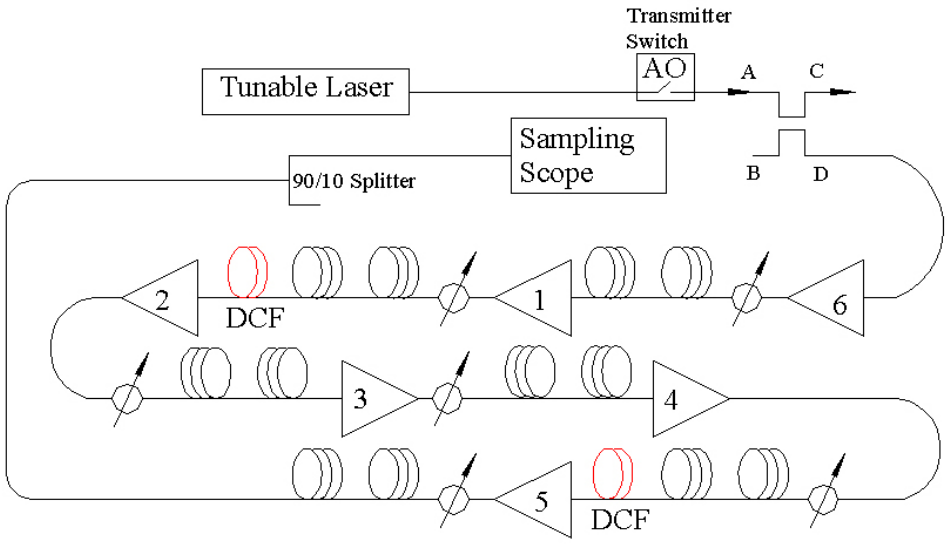

Figure 4.3 The setup of measuring dispersion parameter D.

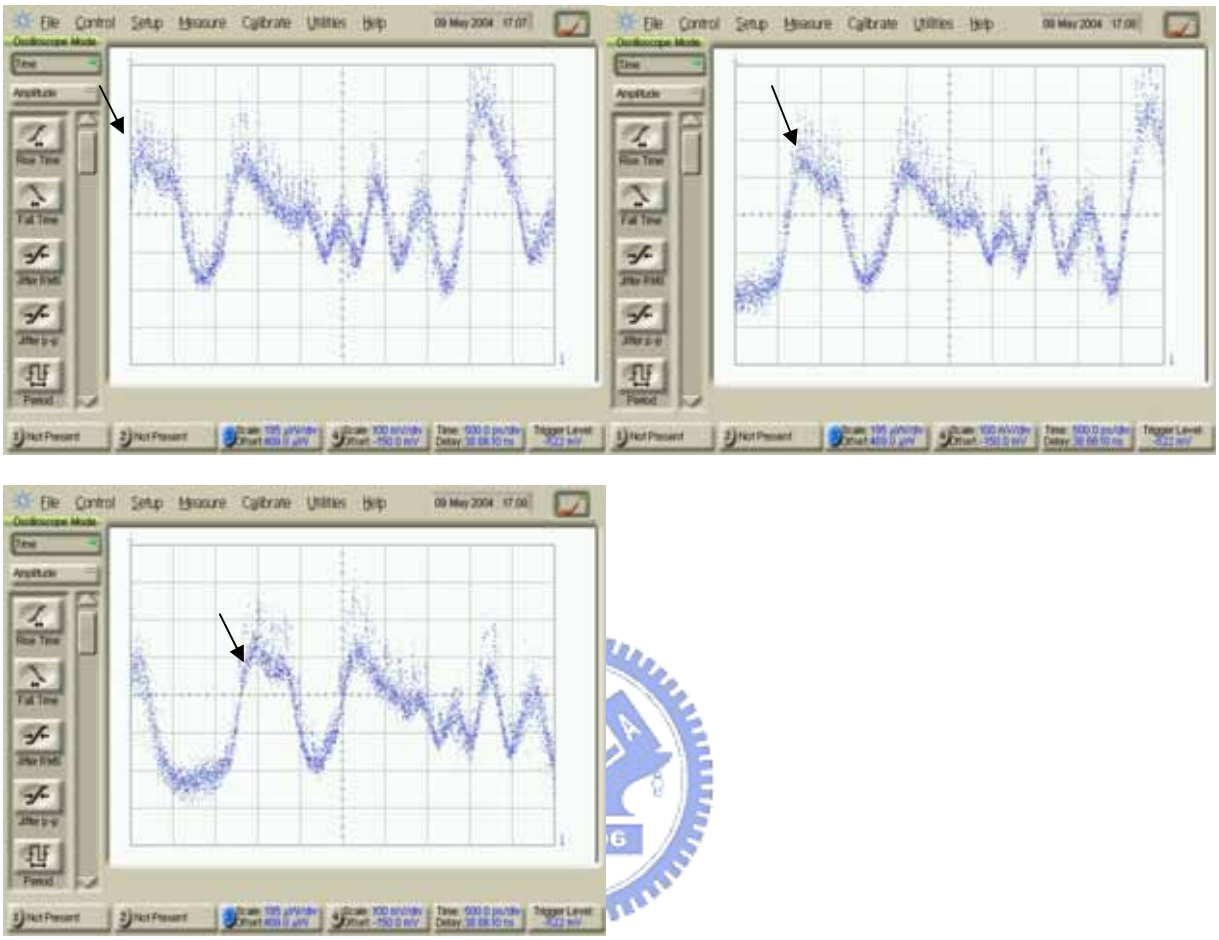

Figure 4.4 The variation of delayed bit stream.

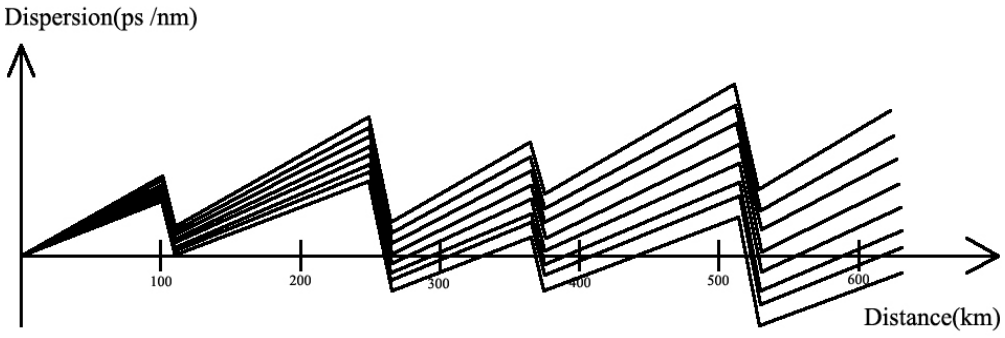

Figure 4.5 The accumulated dispersion versus transmission distance.

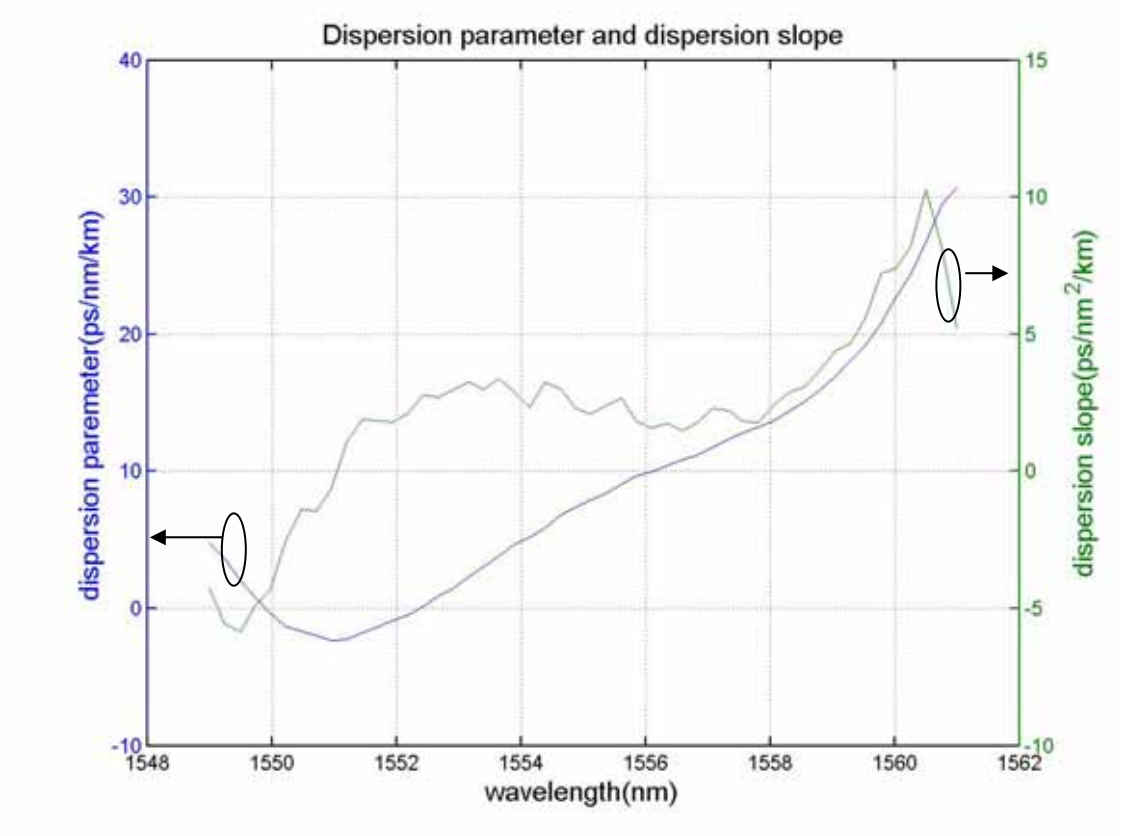

Figure 4.6 The overall dispersion parameter and dispersion slope.

Since different wavelength channels will experience a different total accumulated dispersion after traversing the entire system length, at most one channel will end up with an overall accumulated dispersion of zero after traversing a dispersion managed system. This is seen in the Fig.4.5 by the diverging lines for channels 1 through 8. It results from the nonzero slope of the dispersion curve. The linear approximation for dispersion versus wavelength is

$$D(\lambda) \approx SL(\lambda - \lambda_0) \tag{4.3}$$

where D is dispersion, S is dispersion slope, L is the transmission distance, λ_0 is the zero dispersion wavelength and λ is wavelength. [15]

Chapter 5

Circulating Loop Transmission Experiment

5.1 Line Cascade Six EDFAs

The buildup of amplifier-induced noise is the most critical factor for such systems. There are two reasons behind it. First, in a cascaded chain of optical amplifiers, the ASE accumulates over many amplifiers and degrades the optical SNR as the number of amplifiers increases. Second, as the level of ASE grows, it begins to saturate optical amplifiers and reduce the gain of amplifiers located further down the fiber link. The net result is that the signal level drops further while the ASE level increases. Clearly, if the number of amplifiers is large, the SNR will degrade so much at the receiver that the BER will become unacceptable.

Before we set up our circulating loop experiment, we should test our EDFAs first. We cascade our six EDFAs directly without fiber span. There are attenuators before EDFAs to control the input power of each EDFA. The Fig. 5.1 shows each EDFA have similar gain except the last one. The Fig. 5.2 shows that the output power has fluctuation less than 1dB over the C band with -6 to -14dBm input power. In the operation wavelengths the power varies even less than 0.1dB. The SNR increases with the input power of each EDFA because of the increase on signal power as shown in Fig. 5.3. But the input power can not increase limitless since the nonlinear effect and the degradation of noise figure as shown in Fig. 5.4. The noise figure can be approximated as $2n_{sp}$ for a hypothetical two-level amplifier model with constant populations $N_1 + N_2 = 1$. As the signal level rises, the inversion is depleted, so one expects that the inversion parameter and the noise figure will increase with the signal level. So we choose the -10dBm total input power of each EDFA as the operation

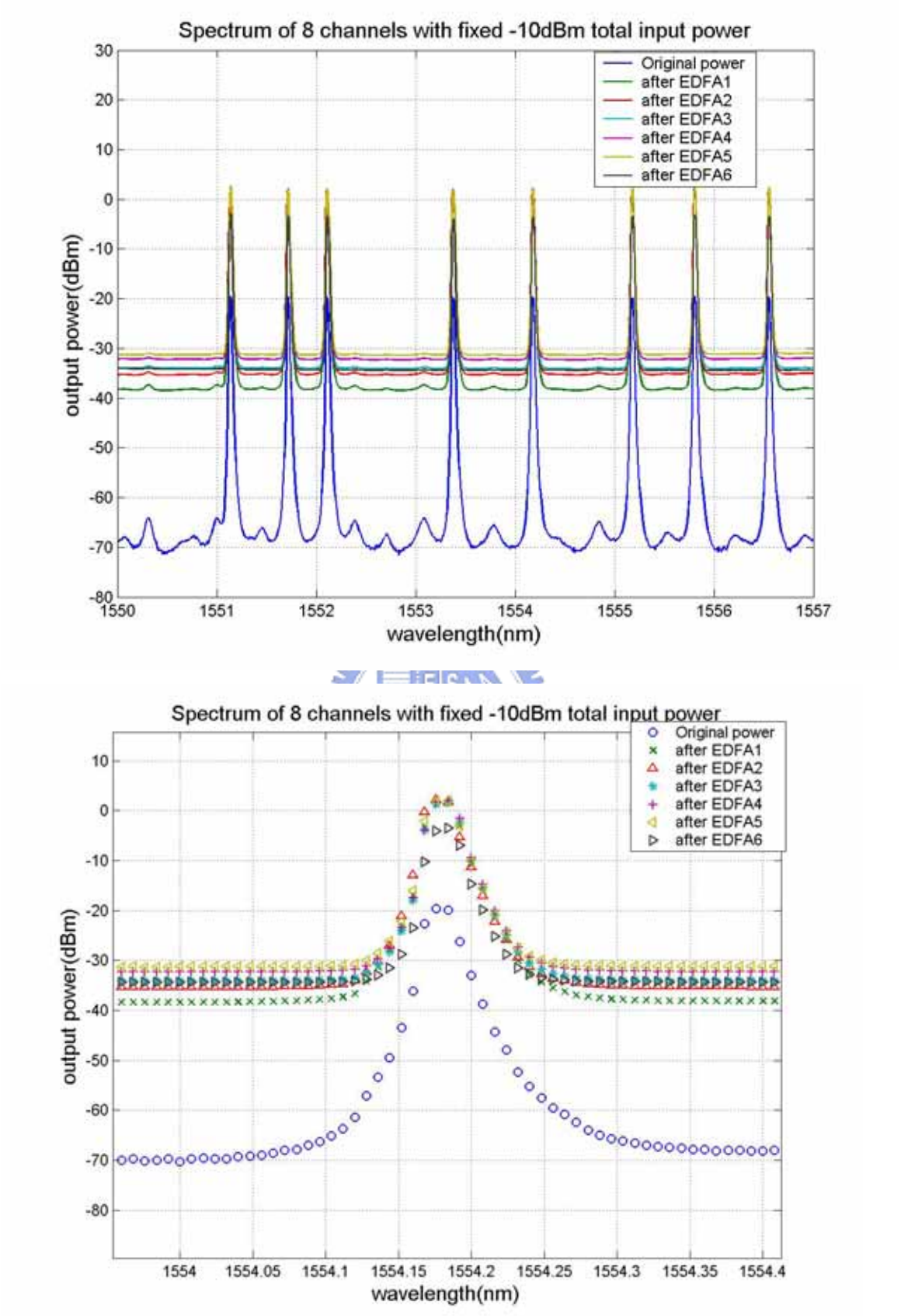

Figure 5.1 Spectrum of 8 channels with fixed -10dBm total input power to each EDFA.

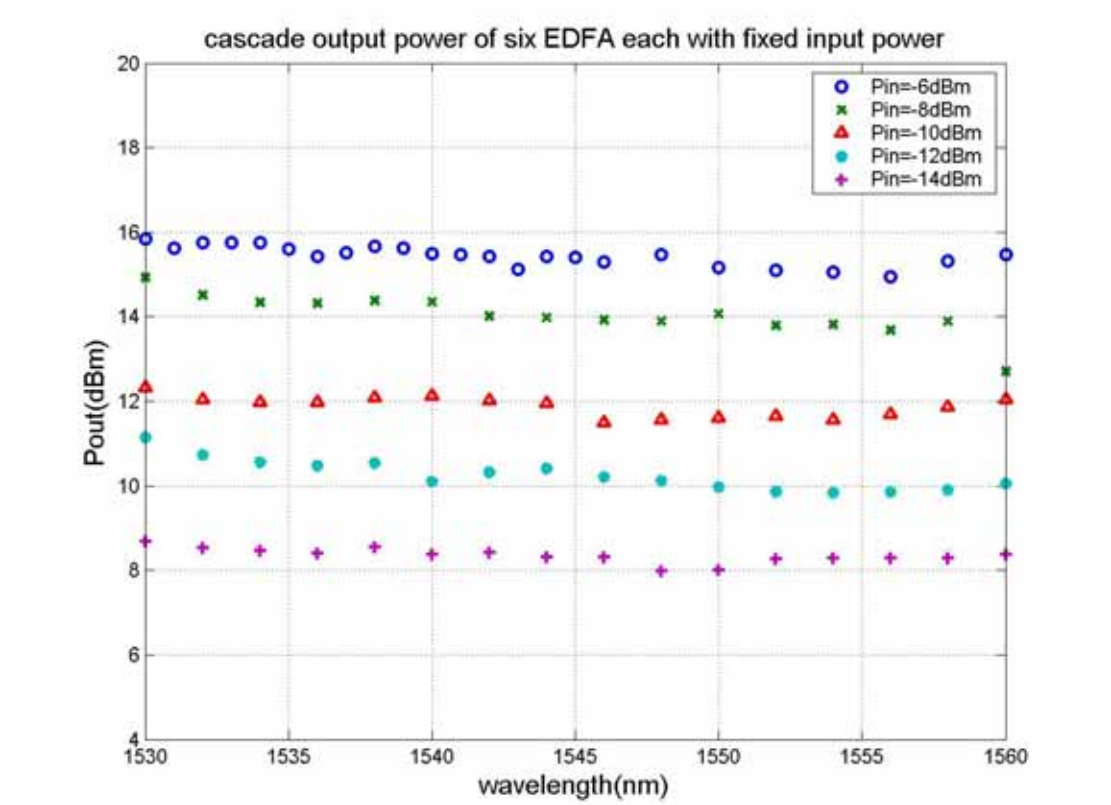

Figure 5.2 Cascade output power of six EDFA with fixed input power to each EDFA.

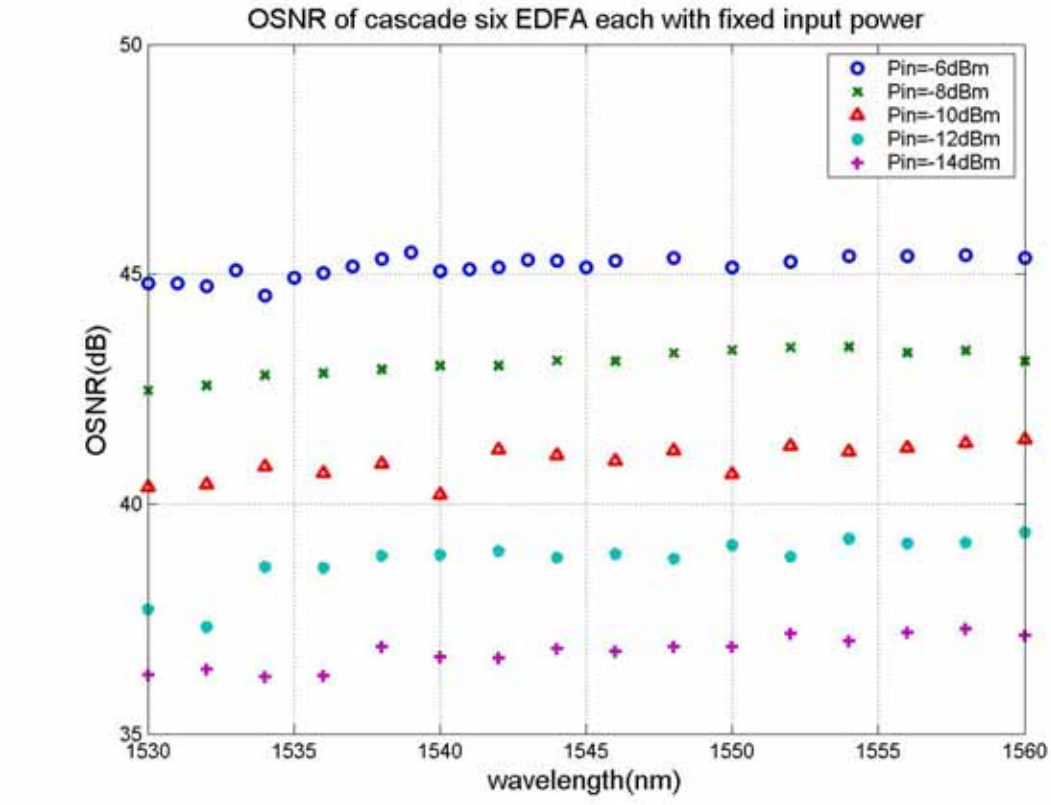

Figure 5.3 SNR of cascade six EDFA with fixed input power for each one.

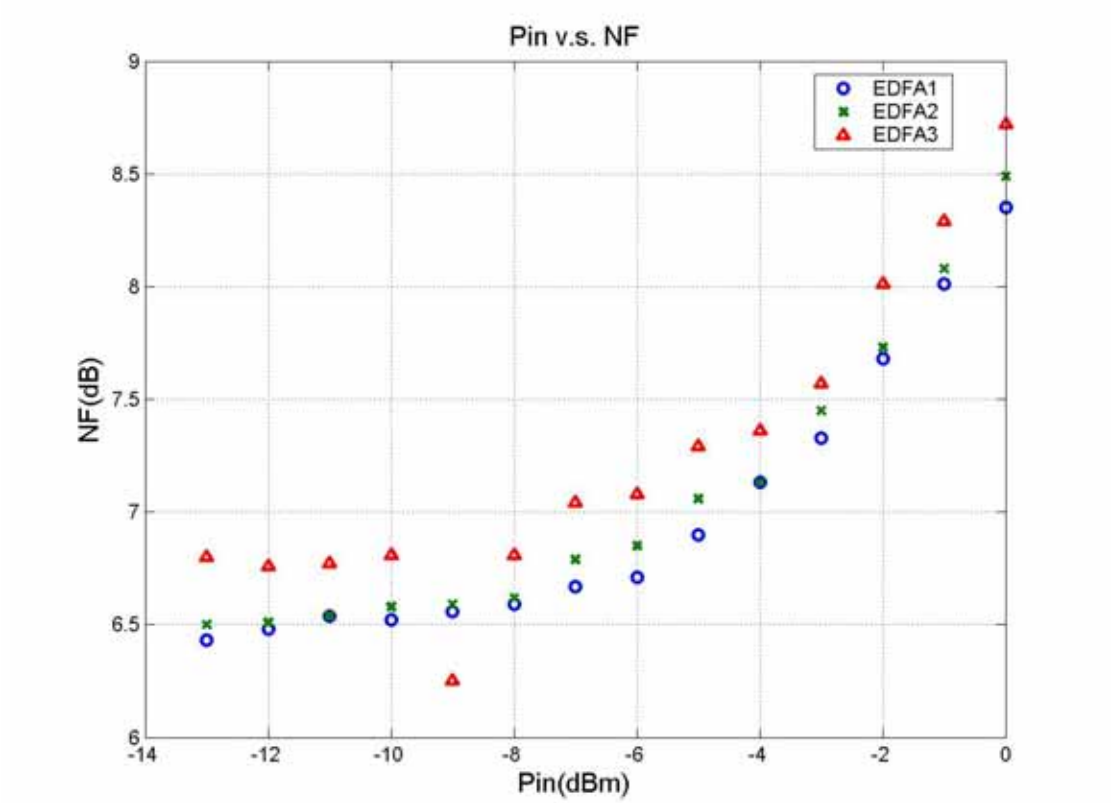

Figure 5.4 Noise figure of three EDFAs.

point.

5.2Gain Peaking

The lightwave systems based on a cascade of inline fiber amplifiers require an understanding of signal gain and noise accumulation along the link. The evolution of the spontaneous emission spectra from cascaded EDFA is shown in Fig. 5.5. The figure shows the ASE of our system has gain peak at 1562nm. Our EDFAs are designed with gain flattening until 1562nm. For a hypothetical two-level amplifier model the gain will be proportional to $N_2\sigma_e(\lambda)-N_1\sigma_a(\lambda)$ and for a well pumped amplifier operating in small signal conditions ($N_1=0$ and $N_2=1$), the gain spectrum has the same shape as that of the emission cross section $\sigma_e(\lambda)$. For an amplifier operating deep in saturation we have $N_1=1/2$ and $N_2=1/2$, in which

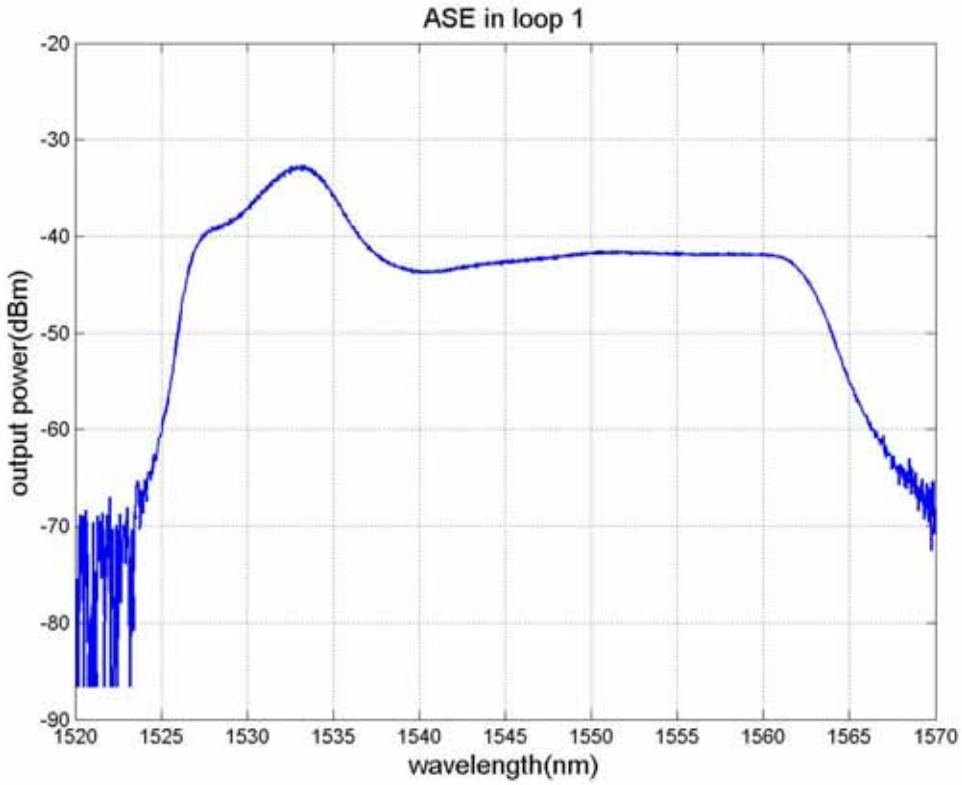
ASE in loop 1
output power(dBm)
wavelength(nm)
-20
-30
-40
-50
-60
-70
-80
-90
1520
1525
1530
1535
1540
1545
1550
1555
1560
1565
1570

(a)

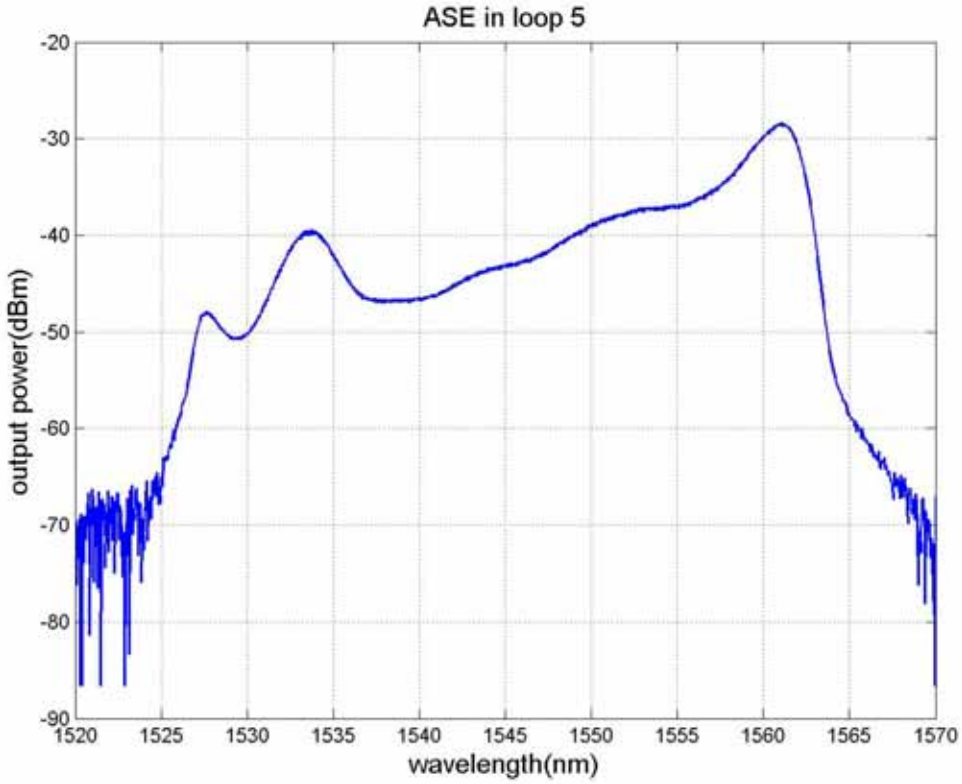
ASE in loop 5
output power(dBm)
wavelength(nm)
-20
-30
-40
-50
-60
-70
-80
-90
1520
1525
1530
1535
1540
1545
1550
1555
1560
1565
1570

(b)

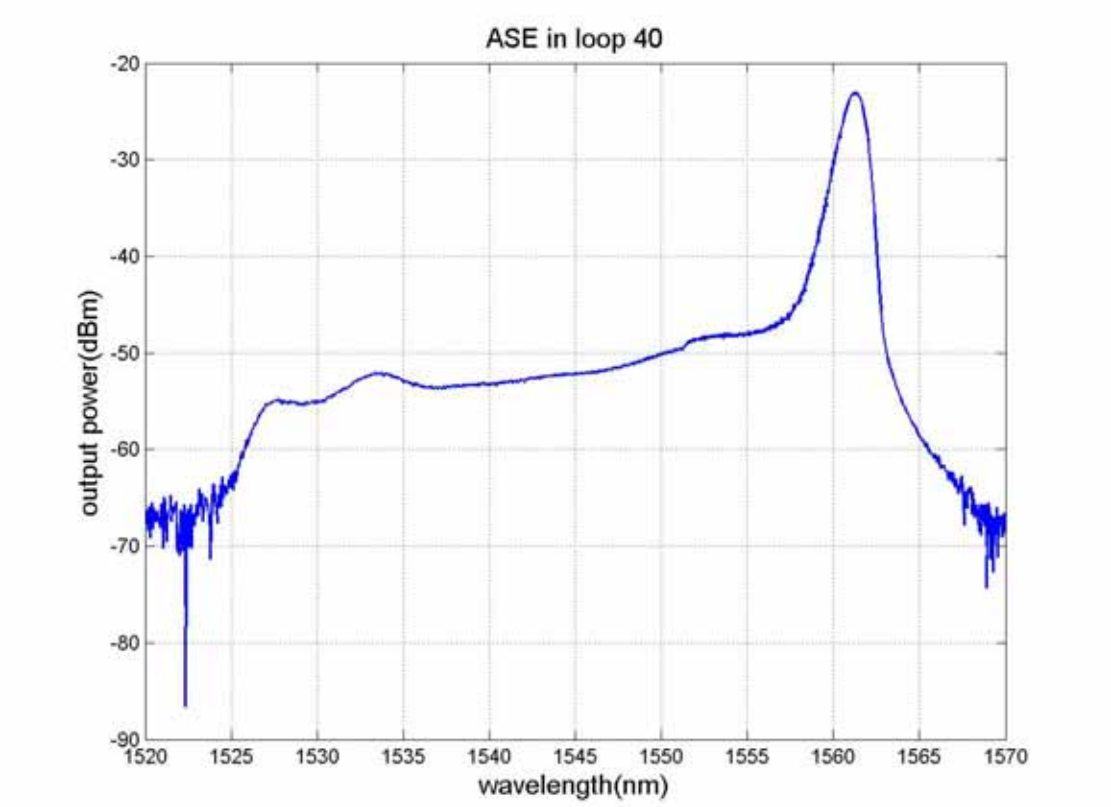

(c)

Figure 5.5 ASE after (a) first loop (b) fifth loop (c) forty loop.

case the gain spectrum is proportional to the difference between the emission and absorption spectra $\sigma_e(\lambda)-\sigma_a(\lambda)$. In most amplifier chains the level of saturation builds up along the chain as the ASE and signal power build up, therefore the individual gain spectra vary with position along an amplifier chain. The amplifier gain peak wavelength has been shown to be determined by the average inversion of the EDFA and the peak gain per unit length. [16] Note also that the fiber loss in the spans between the amplifiers is wavelength dependent and is higher at 1530nm than 1550nm (due to $1/\lambda^4$ dependence of the Rayleigh scattering component of the loss).

Thus, strictly speaking, the spectral variation of the transmitted signal and ASE is a convolution of the fiber spectral loss and amplifier spectral properties. Using phenomenological EDFA modeling parameters, the gain per unit length ($G(\lambda)/L$) for am

amplifier with an average fractional population density in the upper state $\bar{N}_2 / N$ may be expressed as

$$\frac{G(\lambda)}{L} = \{g^*(\lambda)\frac{\bar{N}_2}{N} - \alpha(\lambda)\frac{\bar{N}_1}{N} - l(\lambda)\} \tag{5.1}$$

where $g^*(\lambda)$ is the gain per unit length (dB/m) for the fiber with the erbium ions completely inverted, $\alpha(\lambda)$ is the absorption per unit length (dB/m) when the fiber erbium ions are not inverted, $l(\lambda)$ is the fiber background loss (dB/m), $\bar{N}_2$ is the average upper state population density (along the length of fiber) and N is the total erbium ion density. [16] Equation implies that the gain peak wavelength is independent of pump wavelength, pump power, signal power, amount of gain compression, or amplifier configuration for a given operating gain and fiber length. The Circulating loop configurations have been used with some success to measure the gain peak wavelength. [17][18][19] The gain spectrum of an amplifier chain results from the superposition of the gain spectrum of the individual amplifiers. Even if the individual amplifier gain spectrum is broad, the region near the gain peak is amplified more than other regions, resulting in spectral narrowing after many stages. Equivalently, the emitted spectrum of a multipass loop simulates the concatenation and spectral narrowing of such an amplifier chain. The gain peak of multiple spans of multiple passes through a loop is the same as the gain peak of the amplifier chain. [5]

5.3 Loop Time

The basic time unit for the experiment is the round-trip time of the closed loop. With reference to the timing diagram Fig. 5.6 (a), the experiment starts with the transmitter switch on and the loop switch off.

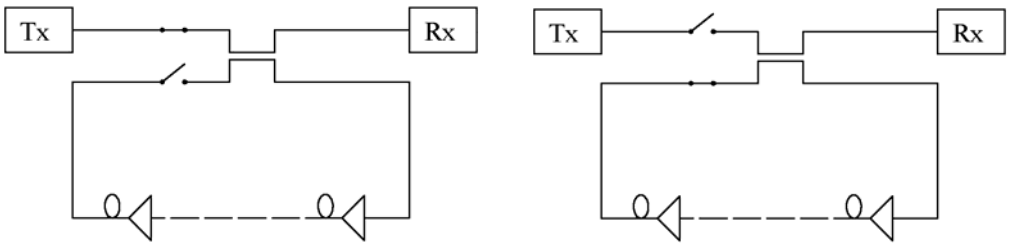

(a) (b)

Figure 5.6 (a) load state (b) loop state.

The two switches are held in this load state for at least one loop time to fill the loop with the optical signals. Once the loop is loaded with data, the switches change state to the loop state as Fig. 5.6 (b), and the data is allowed to circulate around the loop for some specified number of revolutions. A portion of the data signals are coupled to the receiver for analysis. The data signals are received and re-timed by the receiver and compared to the transmitted signal in the BERTS for error detection. The error signals from the BERTS are combined with the error gate in a logic AND gate so that only the errors in the last circulation are counted. The measurement continues, switching between the load and loop states so that errors can be accumulated over long intervals of time. The BER is calculated as the number of errors detected in the error gate period divided by the total number of bits transmitted during the observation period. Since errors are counted only during the error gate period, the effective bit rate for the experiment is diminished by the duty cycle of the error gate signal, thus the real time for demonstrating particular BER might be increased by 50 or 100times over conventional measurements. With an unbroken data pattern, the BERTS still detects errors at the boundaries between each loop time, related the finite speed of the AO switches. During the switch transition from the load state to the loop state, both switches are transmitting some amount of the optical signal. Optical pulses originating from the transmitter will interfere with those pulses returning from the loop, since two pulses have the same

wavelength, but random optical phase and polarization. This interference process corrupts the data bits and causes the BERTS to detect bit errors at the transitions. Since this same signal circulates around the loop, the error bursts are repeated at regular interval of loop time. The synchronization electronics produce a time aperture or error gate for accepting errors, which is a subset of the final loop. The width of the error gate is made smaller than one loop time to avoid the error bursts that occur on the seas of the revolutions.

The circulating loop experiment can be improved upon through the use of bit error detectors with a fast frame synchronization time, usually referred to as burst mode. Here the receiver sees broken sections of the transmitted pattern at each circulation because the data words do not fit evenly into the loop. At each border between circulations, the error detector must reacquire frame synchronization, thus creating a small error burst on the seam. As in the control scheme discussed above, this error burst is removed by gating the error detector and counting only those errors that occur in the middle of the circulation. [12] The description above is shown in Fig. 5.7.

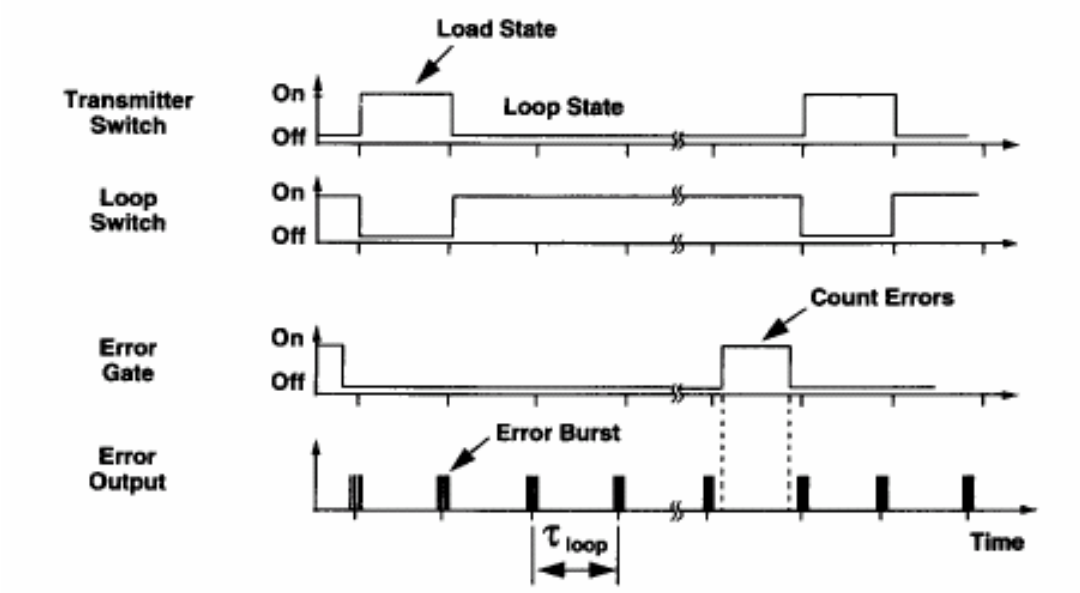

Figure 5.7 The time diagram.

Fig. 5.8 shows the method to measure the round-trip time or called the loop time. We

can get the total power level and its variation after every loop by a low speed oscilloscope as shown in Fig. 5.9. From figure we can see the burst noise comes from the AO switch between every loop. By measuring the interval between every burst noise we can get the loop delay time is about 1.56ms.

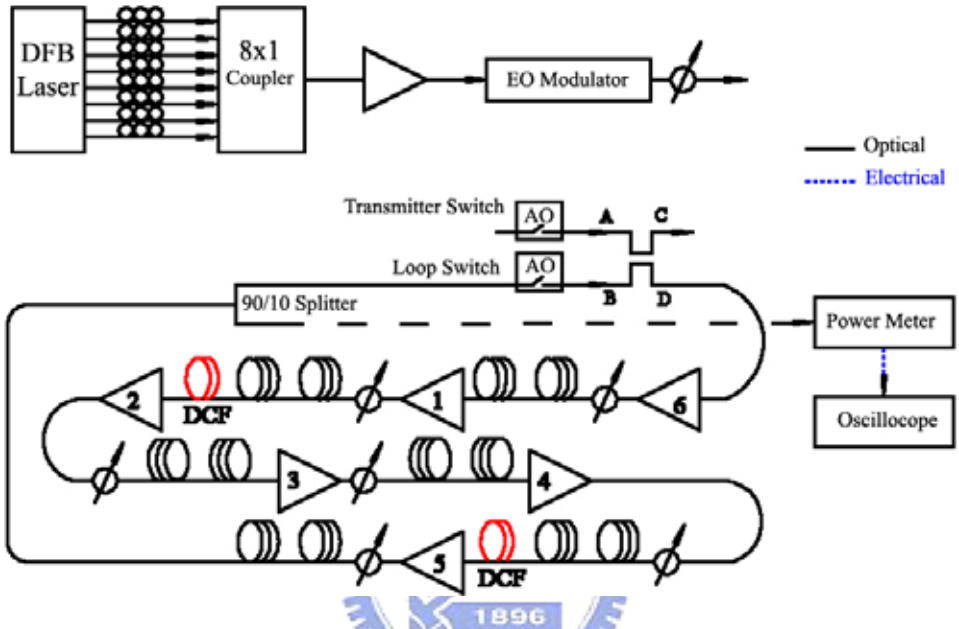

Figure 5.8 The setup for measuring the loop time.

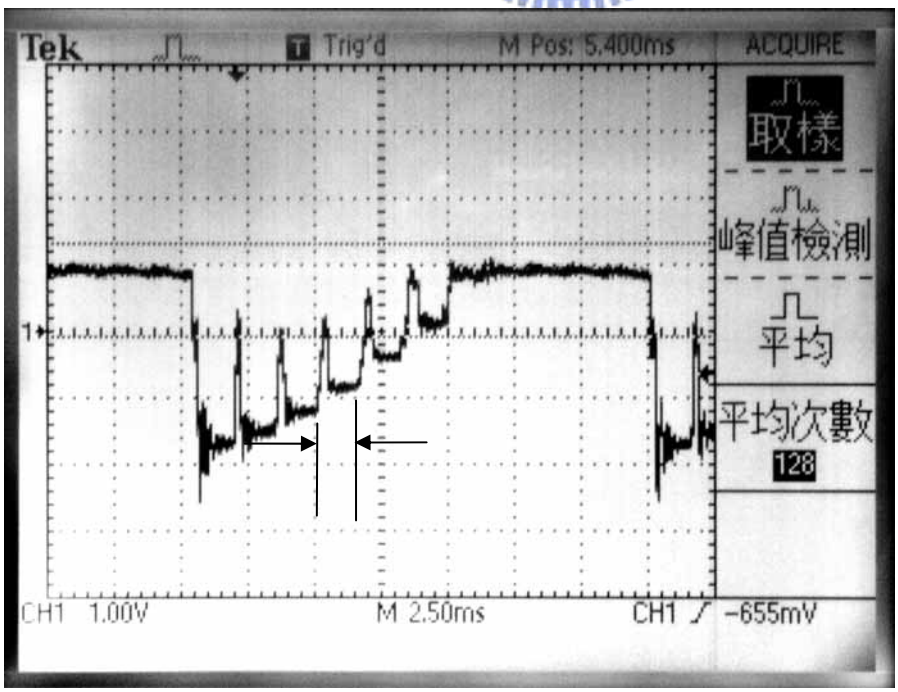

Figure 5.9 The variation of round-trip power.

5.4 Setup

A loop experiment attempts to simulate the transmission performance of a long system by reusing or recirculating optical data signal through a modest length amplifier chain ranging from tens to hundreds of kilometers. [12]

Fig. 5.10 shows the setup of our circulating loop experiment. The eight wavelengths of DFB lasers conform to the ITU channels from 1550.92nm to 1555.75nm with 0.8nm channel spacing.

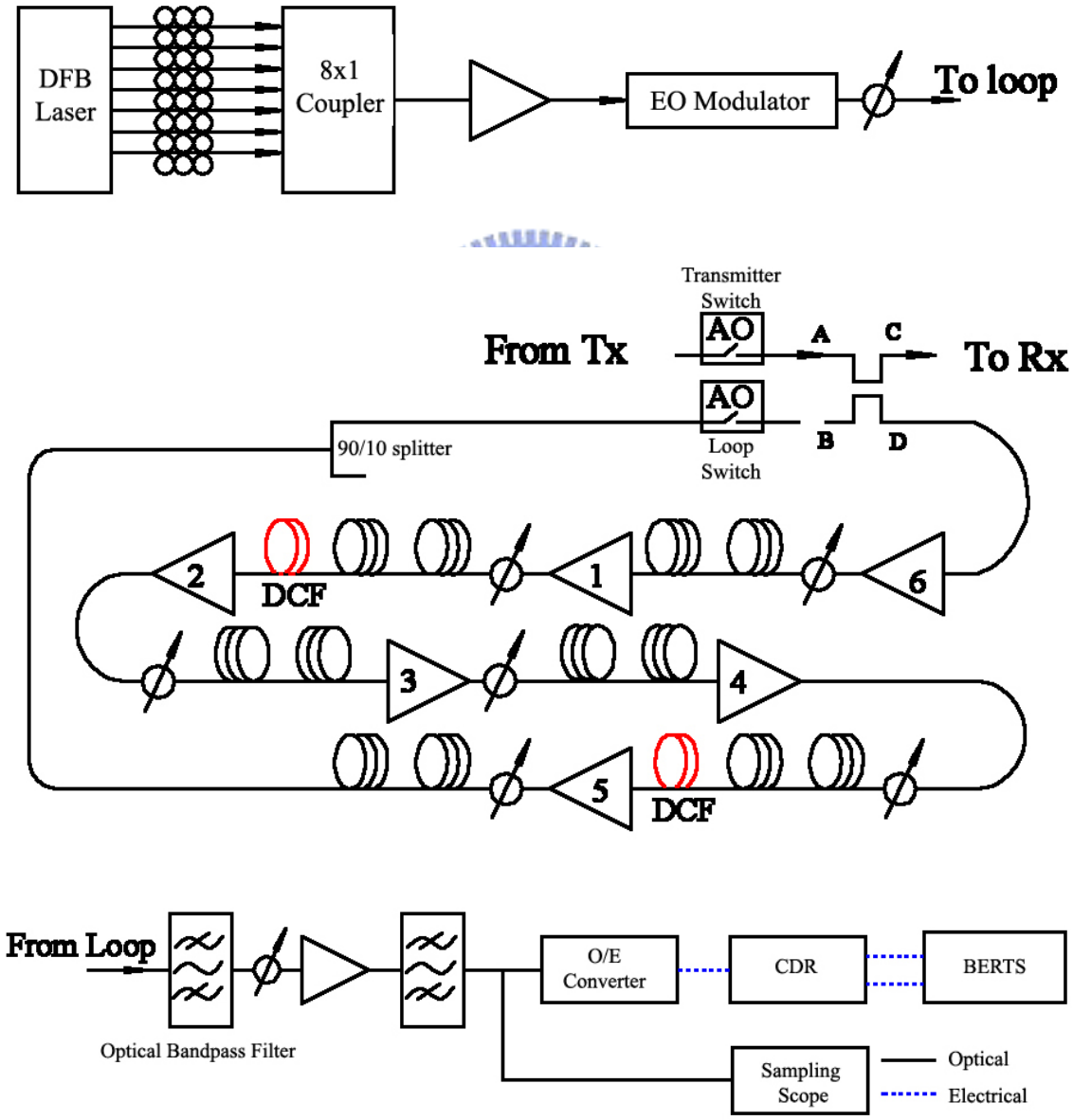

Figure 5.10 The setup of the circulating loop experiment.

There are eight polarization controllers after the DFB lasers to control the polarization of going to the EO modulator. Then the eight channels are coupled into one path by an 8x1 coupler. After the coupler the signals go through the boost EDFA for compensate the loss of coupler. The EO modulator is used for modulating the continuous wave signals into the 10Gbit/s NRZ signals. The signals are coded the $2^{31}-1$ pseudo random binary sequence data patterns. The pulse pattern generator provides the gigabit bit pattern that drives the EO modulator. The data output of the pulse pattern generator must be a high quality eye diagram, that means fast rise and fall time, low distortion, low jitter, and high Q factor. The Anritsu MP1763C has a rise and fall time less than 30ps, less than 10% distortion, less than 20ps peak to peak crossover jitter, and a Q factor larger than 40dB. After the transmitter the signals go through the variable optical attenuator (VOA) to make sure that the signal power before each AO switch and EDFA is the same. In other words, the signals come from the eighth EDFA must the same as which come from transmitter before each AO switch. By adjusting attenuators the loop gain is set to unity. This allows the data to recirculate without loss. The data generator provides synchronizing signals to the transmitter switch, loop switch, and error detector. The AO switches can control when the signals go in the loop and how many round-trips they circulate by the data generator. A 3dB coupler allows for data patterns to be loaded in and also lets them exit the loop after each round-trip. The switching in and out of the data trains needs to be synchronized both with the loop time and the bit error rate test set. The bit error rate after transmission of varying distances can be measured by using the data patterns exiting the loop after the desired number of round-trips, so that any transmission degradation with distance can be observed.

Our loop transmission part consists of six EDFAs (maximum output power=17dBm, fixed gain=22dB and noise figure=6.5dB) followed by 50km of LEAF fiber (D=4.1639ps/nm/km, and loss=0.2dB/km at 1553.33nm) and two DCFs in the appropriate position. Limits to the maximum and minimum power that can be launched into a span are determined by nonlinear

optical effects (4.1) and the noise floor respectively.

The LEAF fiber has large core diameter to reduce the intensity of light and so the nonlinear effect by lifting the threshold of maximum power. Since the fiber loss in one span is less then the gain of EDFA, it needs VOA in each span to attenuate the optical power. For reducing the optical power into the fiber to minimize the nonlinearity the VOA is put just after each EDFA.

The data signals emerging from the loop on the output side of the coupler pass through the appropriate optical bandpass filter and then go into the bit error rate test set.

5.5 Experiment Result

The line width of optical pulse will be broader after modulation. This nature of adding information on carrier source is shown in Fig. 5.11. The line width of DFB laser is very narrow and suitable for WDM system. The optical spectrum can give us the information of OSNR. In the loop the optical power of each channel should be kept constant and the noise floor should be as low as possible. We can see the noise increases as signals propagating as shown in Fig. 5.12, 5.13, and thus the OSNR decreases with distance as shown in Fig. 5.14, 5.15. The channels are closed to the gain peak wavelength, thus the noise floor tilt in long wavelength. Fig. 5.14 shows the worst OSNR after 3000km is still larger than 22dB.

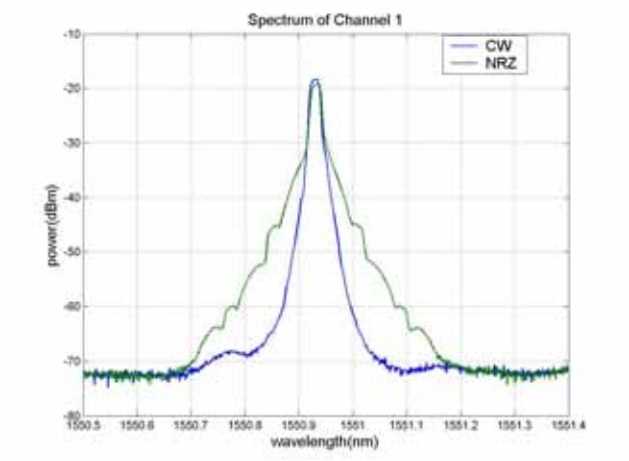

Figure 5.11 The spectrum of channel 1.

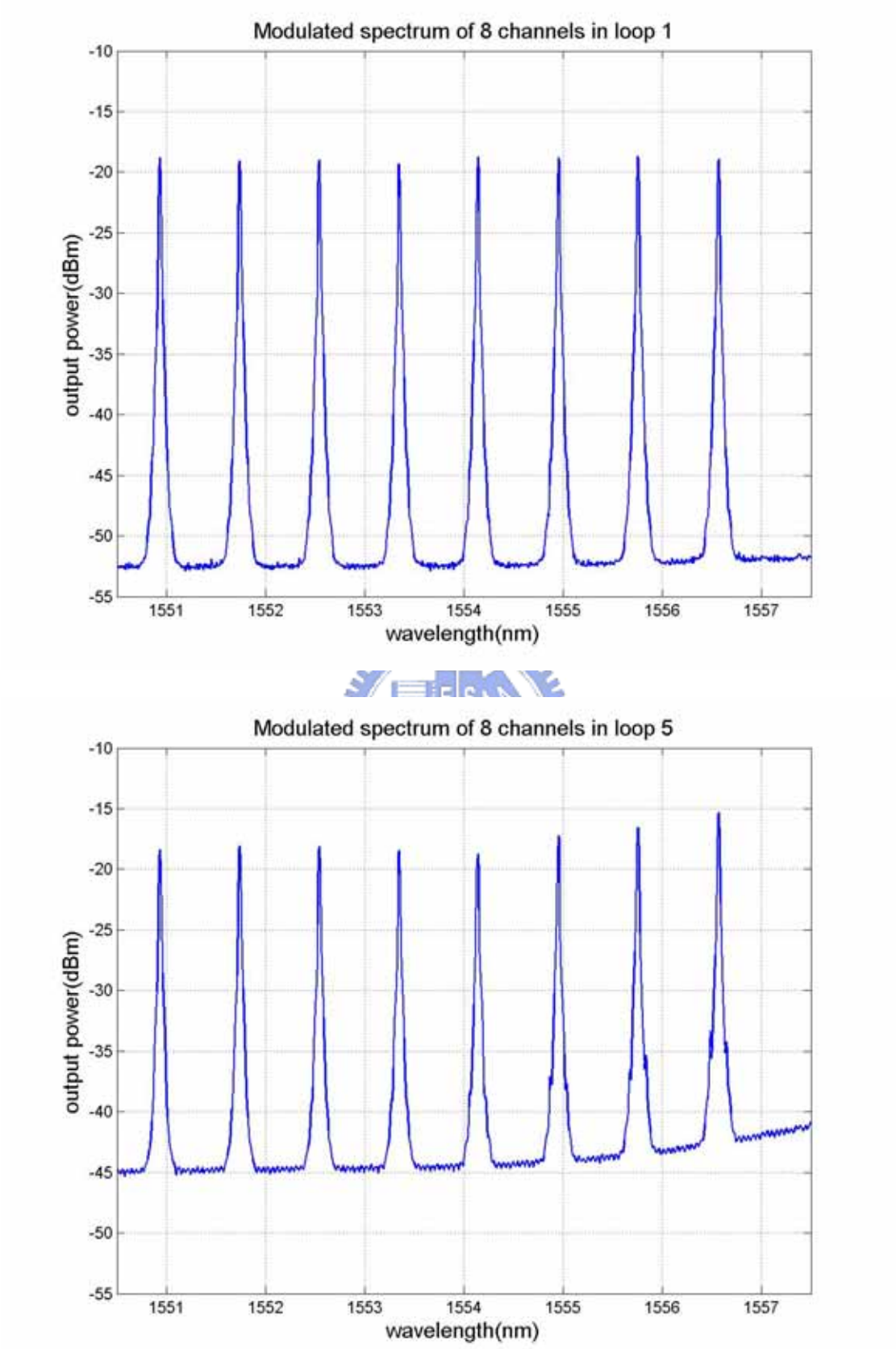

Figure 5.12 The optical modulated spectrum of loop 1 and 5.

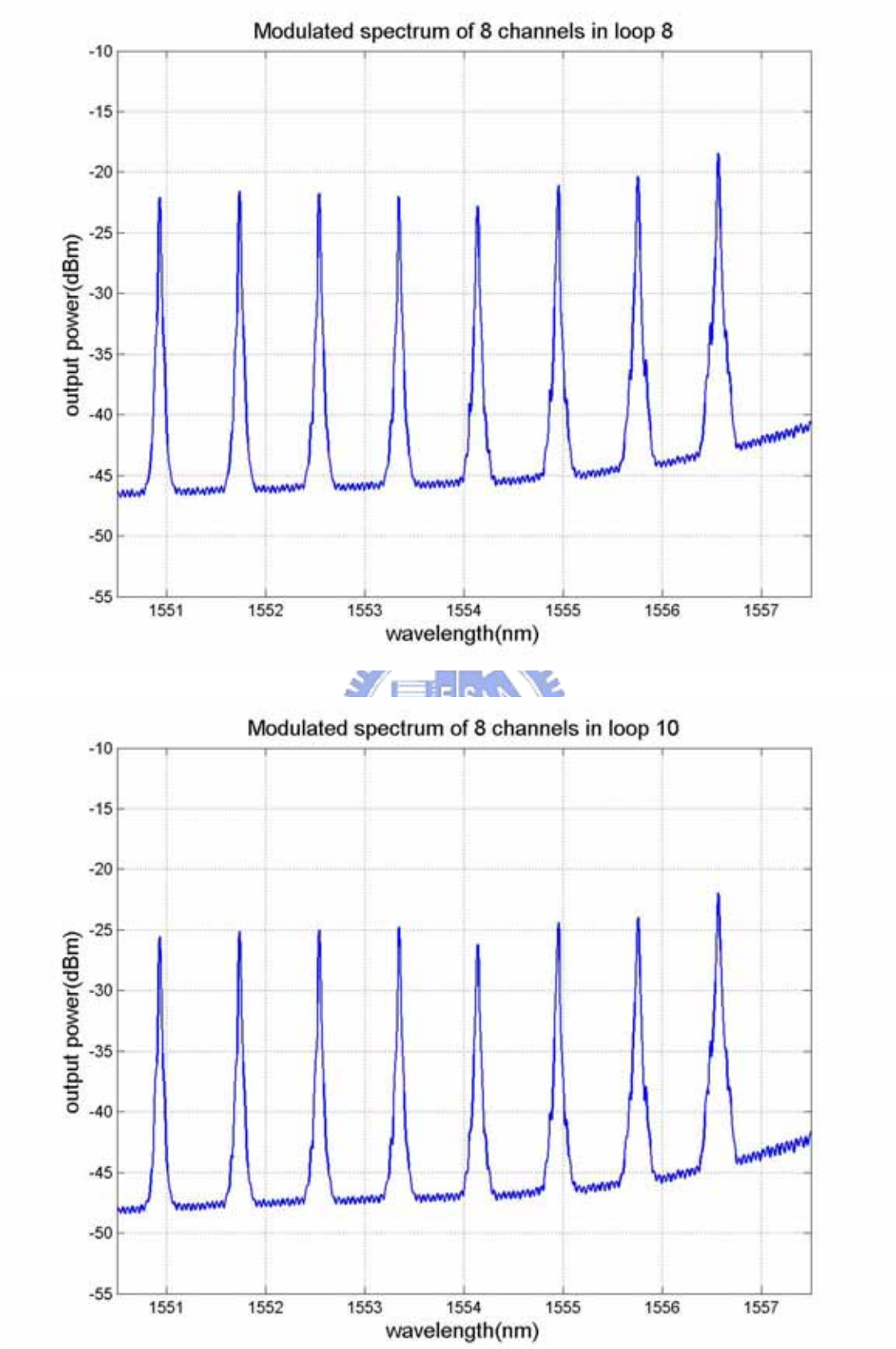

Figure 5.13 The optical modulated spectrum of loop 8 and 10.

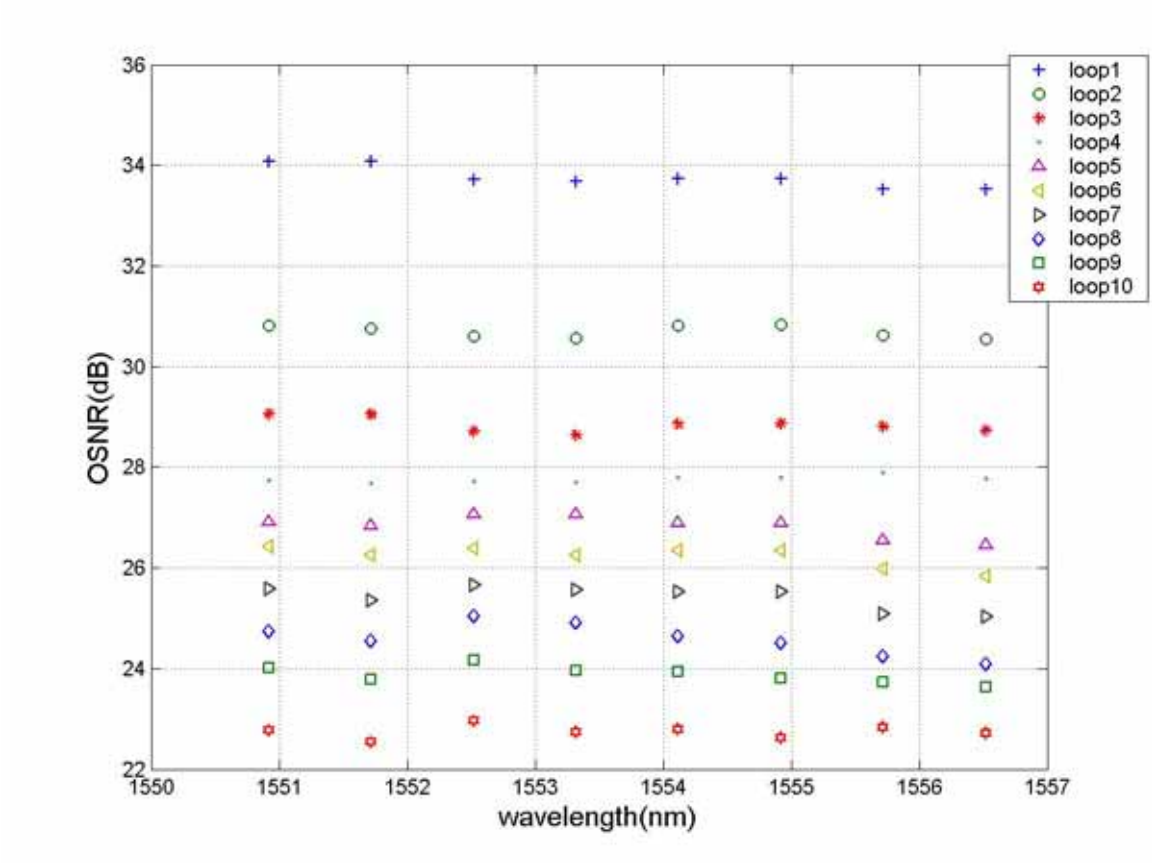

Figure 5.14 The OSNR of eight channels after propagating each loop.

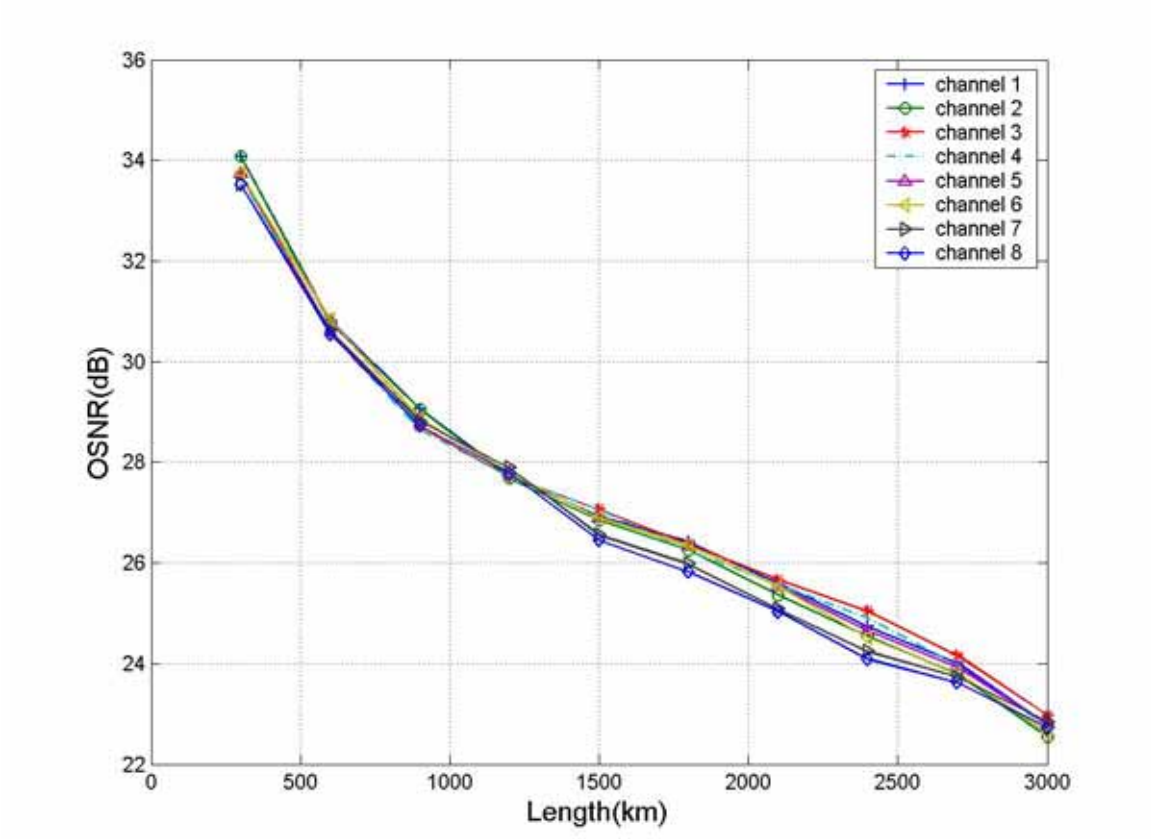

Figure 5.15 The OSNR of eight channels after propagating each loop.

We also measure the BER after one round-trip time. Fig. 5.16 shows the power penalty is about 1dB. We think the reason is about the noise figure of EDFAs. First, the original noise figure of EDFA is too large. Second, for the requirement of circulating loop experiment we close the mechanism of auto-shutdown of EDFA but it will introduces more amplified spontaneous noise because of the always on pump power. The mechanism of auto-shutdown is when there is not input power the EDFA will shutdown. The transmission distance causes the six EDFAs power up and shutdown asynchronous and thus signals can't propagate correctly.

The best eye diagrams measured are shown in Fig. 5.17. They show the noise is too serious to degrade the quality of signals.

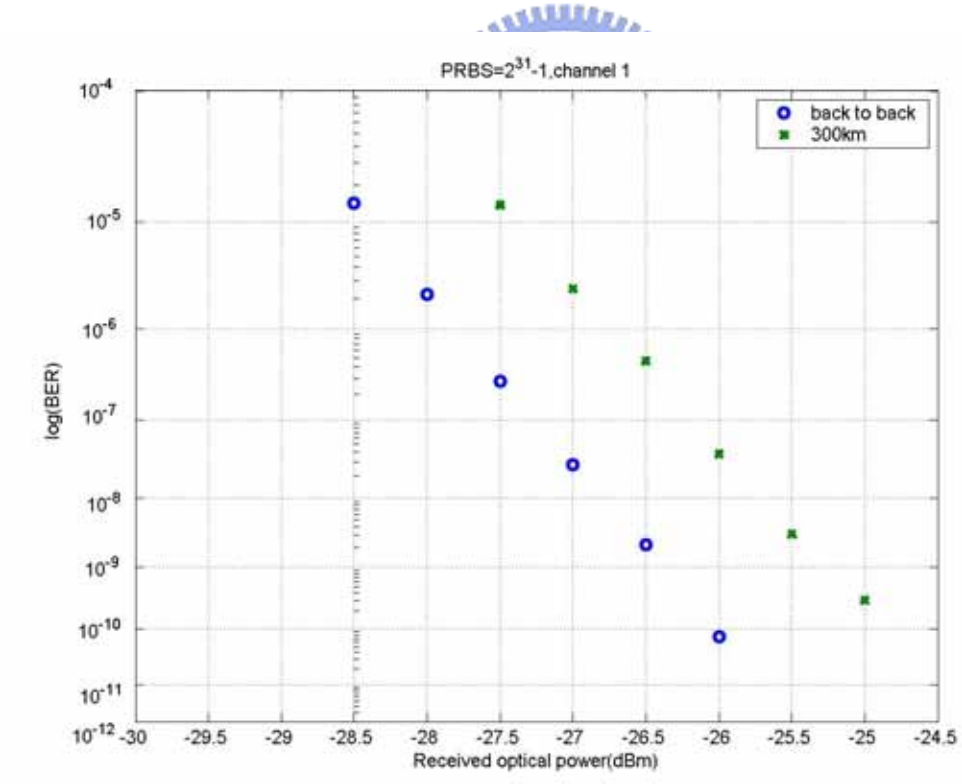

Figure 5.16 BER of back to back and 300km.

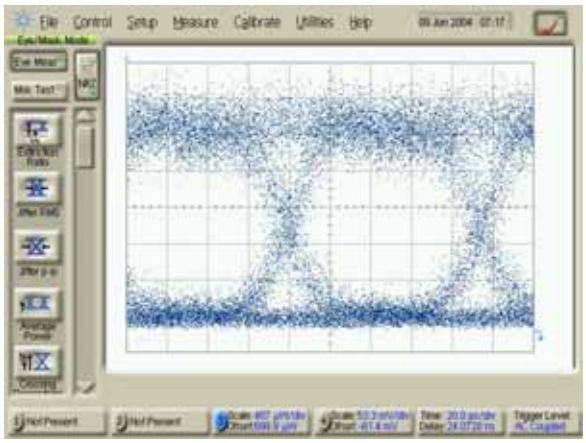

300km

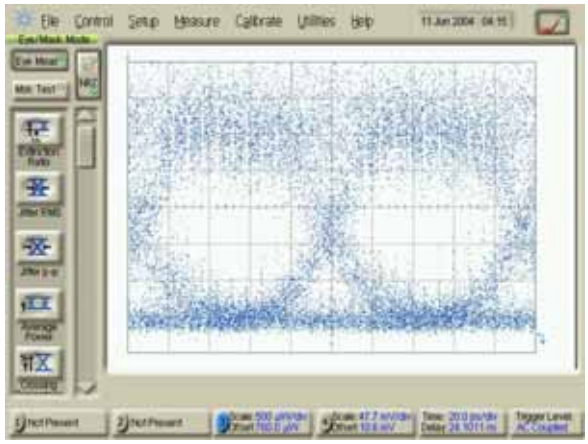

600km

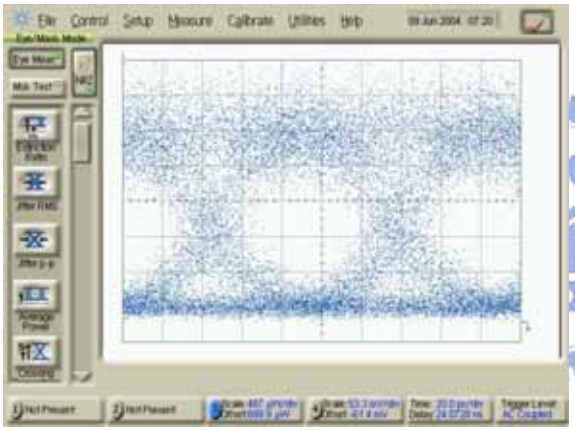

900km

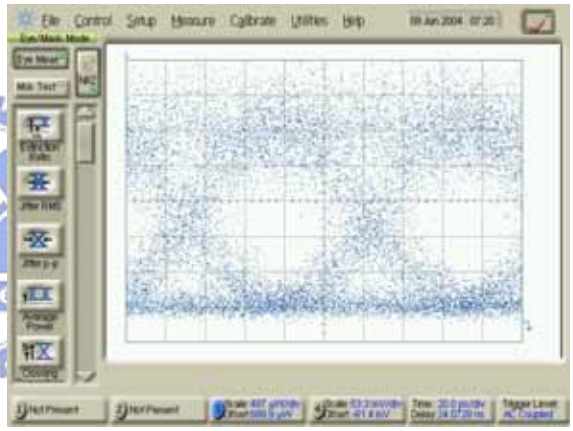

1200km

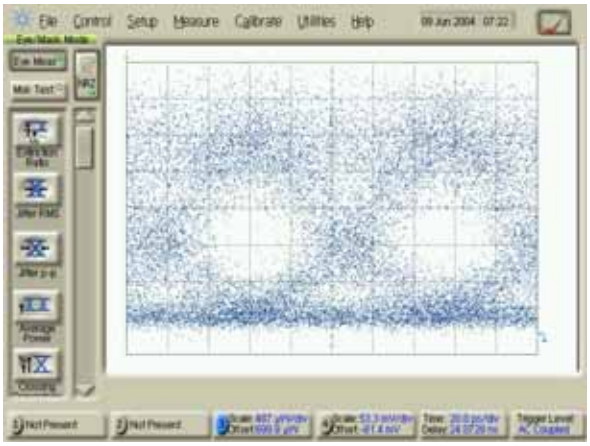

1500km

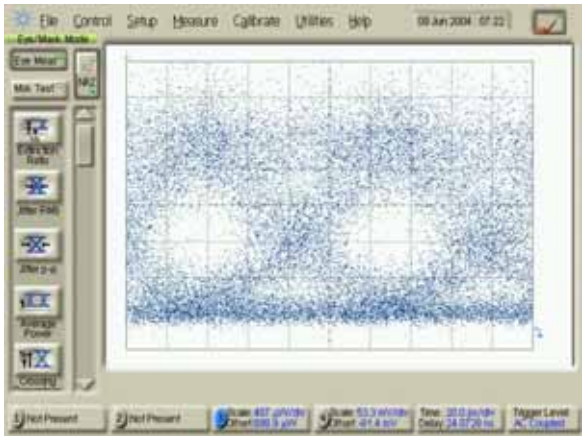

1800km

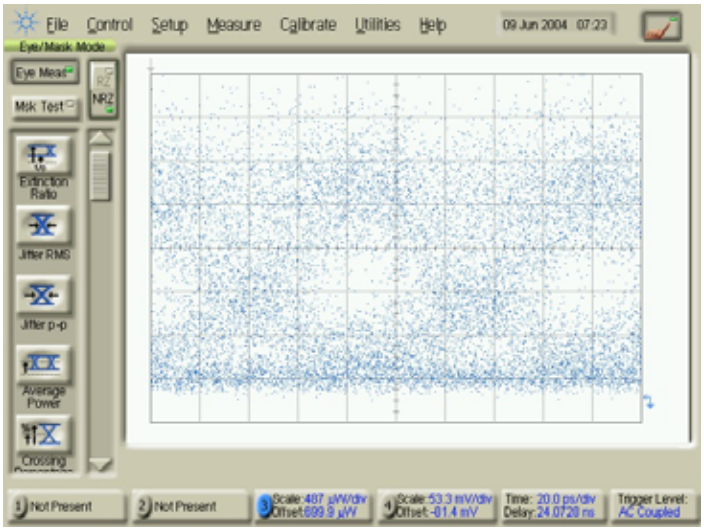

2100km

Figure 5.17 The eye diagram of 300, 600, 900, 1200, 1500, 1800 and 2100km.

Chapter 6

Conclusion

We have accomplished the experimental setup of a circulating loop. By controlling the transmitter switch and loop switch we can allow the signals to circulate in the loop for designate times to simulate the long-haul transmission system. We use the WDM technology to increase the capacity in our experiment. The different wavelengths suffer from different dispersion. We use some DCFs to compensate the accumulated chromatic dispersion and the dispersion slope and yield good results. The SNR after 3000km can still large than 22dB and we believed that by fine tuning the gain and loss of each span and minimizing the amplified spontaneous noise we can get better SNR and thus get longer transmission length.

Bibliography

[1] C. R. Giles, E. Desurvire, J. R. Talman, J. R. Simpson, and P. C. Becker, ”2 Gb/s signal amplification at λ =1.53nm in an erbium-doped single-mode fiber amplifier,” J. Lightwave Technol., vol. 7, no. 4, Apr. 1989.

[2] N. Edagawa, S. Yamamoto, Y. Namihira, K. Mochizuki, and H. Wakabayashi, “First field demonstration of optical submarine cable system using LD-pumped Er-doped optical fiber amplifier,” Electron lett., vol. 25, no. 19, Sept. 1989.

[3] P. Trischitta, M. Colas, M. Green, G. Wuzniak, and J. Arena,”The TAT-12/13 cable network,” IEEE Commun. Mag., vol. 34, pp. 24-28, Feb. 1996.

[4] G. P. Agrawal, “Fiber-Optic Communication Systems,” 3rd ed., John Wiley & Sons, New York, 2002.

[5]P. C. Becker and N. A. Olsson, “Erbium-Doped Fiber Amplifiers Fundamentals and Technology,” New Work: Academic, 1999.

[6]L. F. Mollenauer and K. Smith,” Demonstration of soliton transmission over more than 4000km in fiber with periodically compensated by Raman gain,” Opt, Lett. 13, no. 8, p. 675, 1998.

[7] P. M. Morse and H. Feshbach, “Methods of Theoretical Physics,” McGraw-Hill, New York, 1953, Chap. 9.

[8]G. P. Agrawal, “Nonlinear Fiber Optics,” 2nd ed. New Work: Academic, 1995.

[9] Harry J. R. Dutton,” Understanding Optical Communications,” New York: Academic, 1988.

[10] A. Yariv and P. Yeh, “Optical Waves in Crystals,” John Wiley & Sons, New York, 1984.

[11] “Introduction to Acoustco-Optics,” Brimose.

[12] N. S. Bergano and C. R. Davidson,” Circulating Loop Transmission Experiments for the Study of Long-Haul Transmission Systems Using Erbium-Doped Fiber Amplifiers,” J.

Lightwave Tech., 13, 879, 1995.

[13] M. I. Hayee, A. E. Willner, “NRZ Versus RZ in 10-40-Gb/s Dispersion Managed WDM Transmission systems,” IEEE Photon. Tech. Lett., Vol. 11, No. 8, Aug. 1999.

[14]P. Kaiser and D. B. Kech,”Fiber types and their status,” in Optical Fiber Telecommunications II, New York: Academic, 1988, ch. 2

[15] N. S. Bergano and C. R. Davidson,” Wavelength Division Multiplexing in Long-Haul Transmission Systems,” J, Lightwave Tech, 14, 1299, 1996.

[16]P. F. Wysocki, J. R. Simpson and D. Lee, IEEE Photon. Tech. Lett., 6, 1098, 1994.

[17] P. Blondel, J. F. Marcerou, J. Auge, H. Fevrier, P. Bousselet, and A. Dursin,“Erbium-doped fiber amplifier spectral behavior in transoceanic links,” in Optical Amplifiers and Their Applications, vol. 13, 1991 OSA Technical Digest Series(Optical Society of America, Washing ton, D.C.,1991),pp.82-85.

[18] J. P. Blondel, A. Pitel, and J. F. Marcerou,“ Gain-filtering stability in ultralong distance links,” in Conference on Optical Fiber communication, Vol. 4, 1993 OSA Technical Digest Series (Optical Society of America, Washington, D.C., 1993),pp. 38-39.

[19] B. M. Desthieux, M. Suyama, and T. Chikama, “Self-filtering characteristic of concatenated erbium-doped fiber amplifiers,” in Optical Amplifiers and Their Applications, Vol. 14, 1993 OSA Technical Digest Series(Optical Society of America, Washington, D.C., 1993),pp. 100-103.